Calcareous nannofossil biostratigraphy and biochronology across the Eocene-Oligocene transition: the record at IODP Site U1509 (Tasman Sea) and a global overview

Allyson Viganò[a*], Edoardo Dallanave[b], Laia Alegret[c], Thomas Westerhold[d], Rupert Sutherland[e], Gerald R. Dickens[f], Cherry Newsam[g], Claudia Agnini[a]

[a] Dipartimento di Geoscienze, Università di Padova, Padova, Italy

[b] Faculty of Geosciences, University of Bremen, Bremen, Germany

[c] Departamento de Ciencias de la Tierra & IUCA, Universidad de Zaragoza, Zaragoza, Spain

[d] Center for Marine Environmental Sciences (MARUM), University of Bremen, Bremen, Germany

[e] School of Geography, Environment and Earth Sciences, Victoria University of Wellington, Wellington, New Zealand

[f] Trinity College Dublin, The University of Dublin College Green, Dublin, Ireland

[g] Network Stratigraphic Consulting Ltd., Harvest House, Cranborne Road, Potters Bar, EN6 3JF, UK

[*]Corresponding Author: Allyson Viganò, allyson.vigano@phd.unipd.it, +390498279187, +390498279134.

Abstract

The abundance, wide distribution, and high evolutionary rates of calcareous nannofossils provide a powerful and reliable tool for correlating and dating marine sedimentary records, especially during the Cenozoic. Their assemblage turnover has been documented extensively across the Eocene-Oligocene transition (EOT), but without a parallel framework toward detailed biostratigraphy. We present highly resolved semiquantitative calcareous nannofossil data from a continuous Eocene-Oligocene transition record recovered during International Ocean Discovery Program (IODP) Site U1509 (Expedition 371), presently located at 34.4° S latitude in the New Caledonia Trough (Tasman Sea). We present an improved age model for sedimentation at this site based on integrated bio-magnetostratigraphy. Our high resolution biostratigraphic data provide an independent age calibration for biohorizons, both established and additional, which we compare to previous biochronological estimates from low-middle and high latitudes. This allows for a critical evaluation of the accuracy, reliability, synchroneity or diachroneity of each biohorizon across different oceanographic domains. Finally, we infer that Site U1509 belonged to the subtropical low-middle latitude domain during the late Eocene to early Oligocene, with a paleolatitude of ~45°S. This result has important implications for paleoceanographic reconstructions.

Keywords: calcareous nannofossils, biostratigraphy, biochronology, Eocene-Oligocene transition, IODP Site U1509

1. Introduction

Calcareous nannofossils provide a powerful stratigraphic tool for Mesozoic (Bown, 1998) and Cenozoic (Agnini et al., 2017) marine sediments and sedimentary rocks. Classical Cenozoic biozonation schemes (e.g., Martini, 1971; Okada & Bukry, 1980), while widely used and appropriate in many instances, suffer from several pitfalls, primarily relating to ambiguous taxonomic concepts and variable reliability of biohorizons. Moreover, the low degree of standardization in counting methods and inconsistent nomenclature definitions have resulted in low quality data that are difficult to correlate (Agnini et al., 2017). Through intensive study of numerous marine records, the taxonomy, abundance patterns, diachroneity and correlatability of index species can elucidate temporal relationships across intervals of paleoceanographic change. Significant refinements in calcareous nannofossil biostratigraphy, has emerged over the last few decades. However, the Eocene-Oligocene Transition (EOT), a ~ 500 kyr interval characterized by a decrease in global temperatures and inception of permanent Antarctic ice sheets (Zachos et al., 2001, 2008; Coxall and Pearson, 2007; Westerhold et al., 2020, Hutchinson et al., 2021), remains understudied.

Changes in past oceanography and climate affected calcareous nannoplankton evolution and diversity through time (Bown et al., 2004) and thus semi-quantitative calcareous nannofossil biostratigraphy spanning the EOT provides insight to answer these questions: which bioevents can be adopted for accurate and reliable correlation of widespread sedimentary sequences? Are there additional calcareous nannofossil datums not utilized that can be used for such purpose? Are there systematic differences between similar paleoenvironments, such as shallow-water and deep-water? How can spatial and temporal heterogeneity in calcareous nannofossils be explained? To address these questions, quantitative analyses of calcareous nannofossil taxa are needed from multiple locations across the oceans. However, at many deep-sea sites, incomplete records span the EOT, presumably a consequence of major oceanographic change (Kennett, 1977).

In 2017, International Ocean Discovery Program (IODP) Expedition 371 unexpectedly recovered an expanded late Eocene – early Oligocene section at Site U1509 on the southwest flank of New Caledonia Trough (**Figures 1, 2**) where sediments appear to have accumulated in an isolated seabed depression at bathyal water depths (Sutherland et al, 2018, 2019a). Crucially, calcareous nannofossils are well preserved and the paleomagnetic signal is easily interpreted, offering an opportunity to couple calcareous nannofossil variations and polarity chrons directly.

The stratigraphic record at Site U1509 is suitable for improving the biostratigraphic and biochronological framework of calcareous nannofossils during the late Eocene and early Oligocene, specifically from Chron C15n to the upper part of Chron C12r (35.29 to 30.57 Ma; CNE19-CNO3) (Agnini et al., 2014). In this study we aim to: (1) investigate standard and additional calcareous nannofossil biohorizons at Site U1509; (2) obtain an improved bio-magnetostratigraphic framework at this site and, in turn, a refined age model; (3) compare, on a common time scale (GTS20; Gradstein et al., 2020) the available biochronologic data from low to high latitudes; and, (4) evaluate the accuracy and significance of bioevents in terms of spatial context and synchronicity. To achieve these goals, our high-quality data are compared with existing records from the

Indian, Equatorial Pacific, North Atlantic, South Atlantic and Southern Oceans to obtain a global biochronological framework. This correlation allows assessing the possible presence of latitudinal inconsistencies (e.g., diachrony, paleobiogeographic provincialism and/or regional constraints) that would in turn provide insights on the Eocene-Oligocene climate evolution.

From the outset, we note that precision of age estimates for bioevents depends on several factors. These include local mass accumulation rate and sampling resolution (which affect the time spanned between successive analyses), the counting methods (where quantitative counts are preferred), the intrinsic quality of each datum (e.g., likelihood of recovery), and most importantly, a means to determine absolute age (e.g., an assumption of sedimentation rate between Chron boundaries). All these are sources of errors and can affect final age assignment. In addition, we are aware that age estimates based on linear sedimentation rates and magnetostratigraphic tie-points are typically less accurate compared to those obtained using astronomically tuned records (Blaj et al., 2009), because the latter ideally provide age models defined by periodic changes in Earth's orbital parameters (i.e., precession, obliquity and eccentricity) (Berggren, 2001). The optimal solution is to have sections with available cyclostratigraphy capturing subtle variations in accumulation rates (Raffi et al., 2016). However, for most published records, such a chronologic framework is missing, and magnetostratigraphic constraints remain the primary tool to assess global reliability of specific biohorizons (e.g., Gradstein et al., 2020).

2. Background

2.1 Zealandia and Expedition 371

Zealandia is a large (4.9×10^6 km^2) mostly submerged (~94%) continent separated from Australia by ocean crust below the Tasman Sea of the southwest Pacific Ocean (Mortimer et al., 2017). Like present-day, much of Zealandia lay at bathyal depths during the EOT. However, the event seems to be missing or incomplete in many New Zealand sections and at Deep Sea Drilling Project (DSDP) sites. Unconformities across the EOT may represent erosion, resulting from either enhanced bottom currents related and the onset of Antarctic glaciation (Kennett et al., 1972; 1975) or tectonic processes (Sutherland et al., 2017; Etienne et al., 2018).

During IODP Expedition 371, six sites were drilled and cored in Tasman Sea (Sutherland et al., 2018): five on northern Zealandia (Sites U1506–U1510) and one on the eastern Tasman Abyssal Plain (Site U1511). The purpose was to collect sediment and data to understand the complex tectonic evolution of Zealandia and regional paleoceanography through the Cenozoic (Sutherland et al., 2018).

Site U1509 lies ~640 km west of the northern tip of New Zealand on the western margin of the New Caledonia Trough at a present-day water depth of 2911 m (**Figure 2**). Operations at this site consist of a single hole (Hole 1509A) drilled and cored by the rotary core barrel (RCB) method to a depth of 691 m below the seafloor (Sutherland et al., 2019a).

Sediments recovered at Site U1509 belong to two lithostratigraphic units: the overlying Unit I, which comprises ~415 m of Pleistocene to upper Paleocene calcareous ooze, chalk, and limestone, and the underlying Unit II, which comprises ~275 m of Paleocene to Upper Cretaceous claystone. Unit I is further divided into

three subunits: Subunit Ia (~ 100 m of Pliocene to upper Oligocene sediments dominated by calcareous ooze and chalk with varying foraminifera abundances), Subunit Ib (~ 40 m of upper to lower Oligocene greenish-gray calcareous chalk, with dominant nannofossils and common to abundant foraminifera) and Subunit Ic (~275 m of lower Oligocene to upper Paleocene calcareous chalk and limestone with varying amounts of siliceous microfossils and chert nodules). The sedimentary record at this site relates to a long, complex and interesting history of sedimentation at the base of Lord Howe Rise, including an expected lower bathyal to abyssal setting during the EOT (Sutherland et al., 2018, 2019a, 2022; Crouch et al. 2022). Perhaps surprisingly given RCB methods, Site U1509 contains a relatively continuous and expanded record of the EOT, one with an average linear sedimentation rate (LSR) of ~2 cm/kyr (Sutherland et al., 2019a; 2022).

This work focuses on Subunit Ic between 267.31 and 183.31 m core depth below Sea Floor-A (CSF-A). Due to complexities encountered during drilling and coring, different depth scales arise. Here and after in this work, seafloor depths for Site U1509 are expressed in meters CSF-A, which is the distance from the sea floor to a targeted depth within recovered core (https://www.iodp.org/policies-and-guidelines). Subunit Ic is dominated by a calcareous component consisting of calcareous nannofossils with rare to common foraminifera. Biosilica was also found and includes sponge spicules, radiolaria, and silicoflagellates (Sutherland et al., 2019a). The studied interval spans ~5 Myr.

2.2 Compilations of Sites with an E/O interval

The new data from Site U1509 can be compared with published age estimates of late Eocene-early Oligocene calcareous nannofossil events from 12 other locations (**Figure 1**; **Table 1**). Eight of these are from low to middle latitudes: ODP Site 1218 (Equatorial Pacific; Blaj et al., 2009), IODP Site U1333 (Equatorial Pacific; Toffanin et al., 2013); IODP Site U1411 (NW Atlantic; Newsam, 2017), DSDP Sites 522 and 523 (SE Atlantic; Backman, 1987), DSDP Site 516 (SW Atlantic, Wei and Wise, 1989); ODP Site 711 (Equatorial Indian; Fioroni et al., 2015) and ODP Site 756 (Indian Ocean; Viganò et al., 2023). Four of these are from high latitudes: ODP Site 1090 (Agulhas Ridge; Marino and Flores, 2002), ODP Site 689 (Maud Rise; Persico and Villa, 2004), ODP Site 744 (Kerguelen Plateau; Persico and Villa, 2004), ODP Site 748 (Kerguelen Plateau; Villa et al., 2008). Basic information on these sites is provided in **Table 1**; they were selected based on high-quality and well-resolved nannofossil biostratigraphy, availability of coupled magnetostratigraphic data, and different latitudes (low, middle, and high), longitudes, depth and depositional settings. Given geological time scale revisions over the last few decades, age estimates of calcareous nannofossil events at the above sites have been presented on different timescales. We have recalibrated all ages on a common time frame, the Geologic Time Scale 2020 (GTS20; Gradstein et al., 2020), so that proper comparisons can be made across all sites, including Site U1509.

3. Methods

3.1. Calcareous nannofossils

A total of 129 samples from Subunit Ic of Hole U1509A, between U1509A-30R-CCW, 19-20 (267.305 m) to sample U1509A-21R-1W, 30-31 (183.305 m), were prepared using standard techniques (Bown and Young,

1998). Selected calcareous nannofossil index species were analyzed using a transmitted light microscope (Zeiss Axioscope 40), at 1250× magnification, to determine semi-quantitative abundance patterns. Nannofossil biostratigraphic data are based on semi-quantitative analyses obtained by counting the number of specimens of the considered taxon present in 1 mm^2 (n/mm^2; Backman and Shackleton, 1983). Average sampling resolution of the ~84 m-thick study interval is ~66 cm (~40 kyr), but this increases to ~30 cm (~20 kyr) across the EOT.

Bioevents are defined following terminology proposed by Agnini et al. (2014): Base (B) is the lowest occurrence of a taxon; Top (T) is the highest occurrence of a taxon; the Base common and continuous (Bc) are the first common and continuous presence of a taxon; the Top common and continuous (Tc) are the last continuous and common presence of a taxon. This nomenclature has been adopted because, like first and last occurrence data, semi-quantitative abundance fluctuations can be correlated consistently (Agnini et al., 2014). We therefore compared the pattern of abundance of individual taxa, as well as their final extinction or appearance. In this work we also include low-middle latitude calcareous nannofossil zonations of Martini (1971), Okada and Bukry (1980), and Agnini et al. (2014) (**Figure 3**).

3.2. Paleomagnetism

To refine the correlation of Site U1509 with the geomagnetic polarity time scale through the uppermost Eocene and lowermost Oligocene, we collected a total of 43 oriented paleomagnetic cube samples (8 cm^3) in the interval between Cores 34R and 26R of Hole U1509A (299.5–221.35 m CSF-A). Samples were trimmed with a diamond saw from the calcareous chalk of Hole U1509A and oriented using the convention described in Sutherland et al. (2019b). Before any natural remanent magnetization (NRM) analysis, we measured the anisotropy of magnetic susceptibility (AMS) of all cubes with an *AGICO KLY-2* susceptibility bridge, using the 15 positions protocol of Jelínek (1977). The degree of AMS was estimated using the anisotropy degree "Pj" of Jelínek (1981), which progressively increases from 1.0 (i.e., absence of anisotropy) parallel with the fabric magnitude.

To explore vector components of NRM, all samples were subjected to stepwise alternate field (AF) demagnetization with 15 steps from 5 mT to 100 mT, measuring the remanence automatically after each step with a *2G Enterprises* SQUID magnetometer placed in line with the *ASC* AF coil (Mullender et al., 2016). We interpreted the demagnetization data by visual inspection of vector end-points demagnetization diagrams (Zijderveld, 1967), determining the vector components of NRM by interpolating selected vector end-points with principal component analysis (PCA), as proposed by Kirschvink (1980). Paleomagnetic components with interpretable orientation but failing to point linearly toward the origin of the demagnetization axes were isolated averaging the vector end-points with standard spherical mean (Fisher, 1953). As cores were drilled using the rotary core barrel technique, they are unoriented with respect to geographic north. We therefore estimated the average inclination of paleomagnetic directions by using the inclination-only approach of McFadden and Reid (1982).

3.3. Age model

The age model proposed for Site U1509 uses positions of paleomagnetic Chron boundaries as tie-points (**Table 2**), with absolute ages conforming to GTS20 (Gradstein et al., 2020). For the lower part of the studied interval, age estimates of calcareous nannofossil events were calculated by applying a linear interpolation between nearest Chron boundaries. Unfortunately, the 50 m between base Chron C12r and base Chron C12n lacks a well-defined paleomagnetic signature and the base of Chron C12n falls in a 4.45 m coring gap between Cores 20R and 21R (178.55-183.00 m; Sutherland et al., 2019a), (Sutherland et al., 2019a). To obtain ages for the upper depth interval, sedimentation rates were extrapolated from the base of Chron C12r upward.

The assumption of constant that sedimentation rate between magnetic chrons across the EOT at Site U1509 warrant discussion. The EOT sediment type is mostly chalk with 80-90 wt% calcium carbonate, and the siliceous content (clay, and siliceous microfossils such as radiolaria, diatoms, sponge spicules, etc.) is minor. The lower Oligocene and Eocene sections are slightly deformed with average dips in cores of ~20° and stepped microfaults with centimeter-scale offsets of planar or linear features. Local submarine slope instability, which occurred just after the EOT, deformed and exposed/reworked older strata farther up-slope, leading to the presence of some reworked Eocene fossils in the upper Oligocene. Although slight deformation is cause for concern when interpreting the calcareous nannofossil biostratigraphic events of this EOT section, the sediment composition and laminated bedding supports a bathyal pelagic environment with relatively constant sedimentation rate. This interpretation due to the lack of any significant fault surfaces by the 80-100% core recovery obtained across the EOT interval. Beyond this assumption of constant sedimentation rates, it is important to consider that Site U1509 was drilled with the rotary core barrel (RCB) technique, with not full recovery (total recovery of Site U1509 - 462.86 m – is 67%) (Sutherland et al., 2019a).

Linear sedimentation rates (LSRs) were assumed to remain constant between tie points, with an average LSR of 1.5-2.0 cm/kyr for the EOT interval. The inferred position of the Eocene/Oligocene boundary (EOB, 33.90 Ma – GTS20) is extrapolated to 250.085 m, ~ 5 m above the Top of *Globigerinatheka index* (254.31 ± 5.63 m), within calcareous nannofossil Zone NP21 (Martini, 1971), and near the top of Chron C13r (Gradstein et al., 2020) while integrating new and shipboard data (Sutherland et al., 2019a). Biohorizons within magnetochrons are positioned following the approach of Hallam et al. (1985) and the recommendation of Cande and Kent (1992) to use an inverted stratigraphic placement relative to the present, where 0 coincides with the top Chron and 1 to the base of the Chron (Agnini et al., 2007). Age calibrations of important nannofossil bioevents recognized at Site U1509 (**Table 2**) are compared with age estimates from published records (assigned using available Chron boundaries and calibrated with respect to the GTS20) to provide a set of reliable events (SM, Table S1).

4. Results

4.1. Biostratigraphy

The studied interval ranges from 267.305 m to 183.305 m and it spans from Zone CNE19 to Zone CNO3 (Agnini et al., 2014), equivalent to Zones NP20-NP23 (Martini, 1971) and Zones CP15b-CP17 (Okada and Bukry, 1980), in general in good agreement with shipboard data (Sutherland et al., 2019a; **Figure 3**).

Calcareous nannofossils are common to abundant and the preservation varies from moderate to good throughout the study interval. Semi-quantitative abundance data allow us to investigate biostratigraphically significant calcareous nannofossil (CN) events (**Figure 3**) and to extrapolate their ages assuming constant linear sedimentation rates (LSRs) between Chron boundaries (**Table 2**).

We investigated taxa displaying robust and clear abundance patterns and/or taxa that are easily recognizable across this critical interval, analyzing 'standard' biostratigraphic markers and less well documented. These latter ones are characterized by lower abundances and/or significant fluctuations, as for example the acme interval of *Lanternithus minutus* or *Isthmolithus recurvus*. Some of these additional bioevents (e.g., the base of *Sphenolithus akropodus*, the Tc and Bc of *L. minutus*, the Tc of *Clausicoccus subdistichus* gr. and *Isthmolithus recurvus*) have not been systematically tested in different geographical areas and/or depositional settings, and certainly require further investigation.

The Top common of Cribrocentrum reticulatum

Agnini et al. (2014) proposed the Tc of *C. reticulatum* to mark the base of Zone CNE20, enabling the subdivision of the long stratigraphic interval between the Base of *Cribrocentrum isabellae* (base of Zone CNE19) and the Top of *Discoaster saipanensis* (base of Zone CNE21) (**Figure 3**). At Site U1509, *C. reticulatum* reaches a peak of 25 specimens/mm^2 at 265.485 m and then drops sharply upcore (**Figure 4**). The Tc of *C. reticulatum* in our dataset occurs within Chron C15n (0.13 down from top Chron), which is consistent with that reported from the Indian Ocean (Site 711, Fioroni et al., 2015). The Top of this species (T) is synchronous in different low-middle latitude areas (Shafik, 1981; Backman, 1987; Premoli Silva et al., 1988; Wei and Wise, 1989). At high latitudes, this event occurs within C16n as reported by different authors (Wei, 1991; Aubry, 1992; Marino and Flores, 2002; Persico et al., 2012), confirming a strong diachroneity between low-middle and high latitudes (**Figure 5**).

The Top of rosette-shaped discoasterids

The shortly-spaced successive extinctions of rosette-shaped species *D. saipanensis* and *D. barbadiensis* mark the base of Subzone CP16a (Okada and Bukry, 1980), whereas the extinction of *Discoaster saipanensis* defines the base of Zone NP21 (Martini, 1971), which coincides with the base of Zone CNE21 (Agnini et al., 2014) (**Figure 3**). At Site U1509, the Top of *D. barbadiensis* lies 5.10 meters below the Top of *D. saipanensis* (256.960 ± 0.15 m), both within Chron C13r **(Figure 4**). These datums are consistent with published data from low-middle latitude sites (Backman and Hermelin, 1986; Wei and Wise, 1989; Blaj et al., 2009). The extinction of rosette-shaped discoasters is a diachronous event, which occurs at ~40 Ma in high latitudinal settings (Wei and Wise, 1990; Persico and Villa, 2004; Villa et al., 2008; Fioroni et al., 2015) and occurred ~5.5 Myr later in low-middle latitudes (see discussion in Berggren et al., 1995 and references herein) (**Figure 5**).

The acme interval of Clausicoccus subdistichus group

An acme event of *C. subdistichus* has been identified across the EOT at different sites worldwide (Backman, 1987; Coccioni et al., 1988; Marino and Flores, 2002; Hyland et al., 2009; Toffanin et al., 2013; Norris et al.,

2014; Fioroni et al., 2015; Jovane et al., 2015; Newsam, 2017) and recently at ODP Site 756 (Indian Ocean; Viganò et al., 2023). The Bc of this species was used by Agnini et al. (2014) to identify the onset of the 'acme' and the base of Zone CNO1, which corresponds to the lower part of Zone NP21 (Martini, 1971).

The extinction of *C. subdistichus* was also proposed as a zonal marker by Bukry (1973) and Okada and Bukry (1980) to mark the base of Subzone CP16b (**Figure 3**). However, Bukry (1973) pointed out the objective difficulty of distinguishing three different species belonging to genus *Clausicoccus* (i.e., *C. subdistichus, C. obrutus* and *C. fenestratus*) in overgrown assemblages, and underlined the potential bias in the abundance peaks documented in very well-preserved sediments that would account for high abundances.

In this work, *C. fenestratus* and *C. subdistichus* have the same biostratigraphic significance, but *C. subdistichus* is usually more common (up to 12.8% relative abundance of total assemblage within Chron C13n) than *C. fenestratus*, which typically shows sporadic abundances (0-25 n/mm^2) (**Figure 4**). Thus, for biostratigraphic purposes, they can be included into a single informal taxonomic unit, the *C. subdistichus* group concept (Agnini et al., 2014), even though we can consider the contribution of *C. fenestratus* quite negligible.

At Site U1509, this informal group is characterized by high and variable abundances with a marked increase in the number of specimens (reaching ~470 specimens/mm^2) during Chron C13n (**Figure 4**). A large increase in abundance (Bc) of *C. subdistichus* gr. is observed at 250.35 m ± 0.16 m in the upper part of Chron C13r. It corresponds to the highest number of specimens recorded in 1 mm^2 (Δ= 121 n/mm^2, i.e., from 56 to 177 specimens), and it occurs at C13r (0.16), in good agreement with the position of C13r (0.13) reported in Agnini et al. (2014).

Unfortunately, the Bc of *C. subdistichus* gr., which marks the beginning of the acme, is not easy to locate because the increase in abundance at the onset of the acme interval is not always unequivocally identified, although the acme interval of this taxon represents a valuable and unique datum to approximate the Earliest Oligocene Glacial Maximum (EOGM) (Viganò et al., 2023). At Site U1509, the abundance pattern of *C. subdistichus* gr. shows a sharp decline (Tc) from 336 to 5 specimens/mm^2 at 221.560 ± 0.14 m in the lower part of Chron C12r (**Figure 4**). This biohorizon is recorded above the Top of *Ericsonia formosa*, consistent with findings of Backman (1987) and Catanzariti et al. (1997). The Tc of *C. subdistichus* gr., early in Chron C12r, is also recorded at high latitudes and always above the Top of *E. formosa* (Madile and Monechi, 1991). Similarly, in the Equatorial Pacific (Site U1333; Toffanin et al., 2013) and in the South Atlantic (Site 1263; Bordiga et al., 2015), this group seems to be present and common even after the Top of *E. formosa*.

In conclusion, the reversed relative ranking of these two biohorizons, previously reported by Okada and Bukry (1980), seems to be inconsistent with virtually all available data (**Figure 3**). Possible explanations for these inconsistencies are likely related to misleading correlations between T and Tc, which are spaced biohorizons with the latter preceding the former. In addition, low-resolution qualitative data and taxonomic ambiguity may have biased the quality of the datums and caused the reverse ranking found in some studies (e.g. Wise, 1983; Madile and Monechi, 1991). As documented in the Tasman Sea, as well as in above-mentioned cases, the Tc

of *C. subdistichus* gr. is a clear event recorded after the Top of *E. formosa* but additional data is needed to test the reliability of this biohorizon.

In Hole U1334A, stratigraphic range charts document a significant increase in abundance of *C. subdistichus* (Bc) (Bown and Dunkley Jones, 2012) at the EOB. Consistent with the previous datum, a notable increase in abundance of this species (up to 100 n/mm^2) occurs in the upper part of Chron C13r in Hole U1333C (Equatorial Pacific; Exp. 320) (Toffanin et al., 2013). In contrast, only a few sporadic specimens were found in nearby Holes U1331A, U1332A and U1333A (Bown and Dunkley Jones, 2012), but these qualitative data need further inspection.

The Top of Ericsonia formosa

The Top of *E. formosa* formally defines the base of Zone NP22 (Martini, 1971) and Zone CNO2 (Agnini et al., 2014) **(Figure 3**). At Site U1509, this species is quite common in the lower part of the section, decreasing in abundance towards the upper end of its range. Despite the sporadic final distribution, the Top of *E. formosa* was recognized in the lowermost part of Chron C12r (234.300 ± 0.31 m) (**Figure 4**), a datum that is consistent with most of the low-middle latitude data (Backman, 1987; Wei and Wise, 1989; Blaj et al., 2009; Toffanin et al., 2013) (**Figure 5**).

This event is diachronous between low-middle and high latitudes (Marino and Flores 2002; Villa et al., 2008; Fioroni et al., 2012; Persico et al., 2012), with the last occurrence of this species lying within Chron C18 at high latitudes (Berggren et al., 1995).

The Top and the Top common of Isthmolithus recurvus

In the classical biozonations, the Base of *I. recurvus* defines both the base of undifferentiated Zone NP19/NP20 (Martini, 1971) and Subzone CP15b (Okada and Bukry, 1980). However, many authors have pointed out the low reliability of this late Eocene biohorizon. In particular, Agnini et al. (2014) noted that the first occurrence position of this species with respect to magnetostratigraphy is highly inconsistent, ranging from Chron C17n to Chron C15n. Similarly, the final occurrence of this taxon is sporadic and at some sites is difficult to determine. In addition, Bukry (1978) suggested that *I. recurvus* was likely affected by latitudinal thermal gradients, which consequently results in a diachronic extinction if low-middle and high latitudes are compared. At Site U1509, the distribution of *I. recurvus* resulted in uncertain positioning of the Top of this taxon. Instead, the Tc of this species is at 230.555 ± 0.15 m, within Chron C12r (**Figure 4**), quite consistent with data from northern middle latitudes (Martini, 1971), South Atlantic (Backman, 1987) and southern high latitudes (Persico and Villa, 2004; Villa et al., 2008) (**Figure 5**). The Tc of this species appears to be a more reliable bioevent than the Top occurrence.

The acme interval of Lanternithus minutus

Biohorizons based on the abundance pattern of *Lanternithus minutus* are not used to subdivide biostratigraphically the Oligocene, but here we note the potential of this holococcolith as a regional index species. This species was first described from upper Eocene Austrian glauconite sediments (Stradner, 1962), and more recently its common occurrence was reported from middle to upper Eocene sediments from Tanzania

(Dunkley Jones et al., 2008, 2009), with sporadic occurrences at North Atlantic Exp. 342 sites (Bown and Newsam, 2017). The stratigraphic range of *L. minutus* spans from Subzone NP14b (middle Eocene) to Zone NP23 (early Oligocene) (Bown, 2005). We document a remarkable increase in its abundance across the late Eocene - early Oligocene at Site U1509, with maximum values (>100 specimens/mm^2) observed between 246.905 to 223.205 m, within Chron C13n to C12r. At Site U1509, the Bc of *L. minutus* was documented at 244.205 ± 0.30 m, at 0.66 from the top of Chron C13n. The Tc of this species occurs at 224.705 ± 0.30 m within Chron C12r (**Figure 4**). A similar trend has been observed in the Indian Ocean at Site 756 (Viganò et al., 2023) and seems to correlate perfectly with the acme interval observed at Tasman Sea Site U1509. Therefore, we may have identified a useful new biohorizon at the EOT.

The Top of Reticulofenestra umbilicus

The top of *R. umbilicus* is known to be diachronous between low-middle and high latitudes (e.g., Backman, 1987). Following Backman and Hermelin (1986), we only include *R. umbilicus* specimens >14 μm.

In the recent biozonation by Agnini et al. (2014), the extinction of *R. umbilicus* marks the base of Zone CNO3 (**Figure 3**). In our dataset, the abundance pattern of this species displays a progressive decline through time and reworked specimens are present, as highlighted in the shipboard reports (Sutherland et al., 2019a). However, the Top of *R. umbilicus* was placed at 203.395 ± 0.29 m, which coincides with its sharpest decline in abundance and is consistent with a constant LSR (**Figure 4**).

4.2. Paleomagnetism

Generally, sediments from IODP Exp. 371 provide a reliable magnetic remanence signal (Dallanave and Chang, 2020). In Hole U1509A, the AMS of samples possesses a prolate shape in the form of $k_1 \approx k_2 > k_3$, where k_1, k_2, and k_3 are the maximum, intermediate, and minimum axes of the anisotropy tensor, respectively (**Figure 6**). This fabric is confirmed at a site level by the distribution of eigenvalues (v_i) obtained by analysis of 1000 bootstrapped datasets (Constable and Tauxe, 1990): the distributions of v_1 and v_2 overlap and are distinct from v_3 (**Figure 7**). The observed prolate AMS with vertical k_3 is typical of undisturbed sediments and supports the reliability of the paleomagnetic data. This is because drilling-induced deformation or tectonic strain readily affects the shape and orientation of the magnetic susceptibility tensor and possibly the orientation of paleomagnetic directions (Bowles, 2007; Dallanave and Kirscher, 2020).

After NRM analysis of 43 samples we isolated a characteristic remanent magnetization (ChRM) from 37 samples: 29 through PCA interpolation; and 8 using the Fisher (1953) mean approximation. In most cases the ChRM component was isolated between 20 mT and 80 mT **(Figure 7**). The average confidence angle for the whole dataset is 11.7° in case of the PCA-interpolated directions (maximum angular deviation; Kirschvink, 1980) and 9.6° in case of the Fisher mean-approximated directions (α_{95}; Fisher, 1953). Notably, the inclination of the ChRM directions decreases stratigraphically downward from absolute values of ~50° at Core 26R to less than 30° at Core 33R (**Figure 8**). This is likely an artifact of the degree of sediment compaction that increases downward. In fact, the anisotropy parameter Pj also shows an increasing downward trend from values

of ~1 (i.e., negligible AMS fabric) to almost 1.2, the latter overcoming the empirical 1.04 threshold beyond which inclination shallowing of paleomagnetic directions is expected (Li et al., 2014) (**Figure 8**).

Despite relatively high confidence angles, the paleomagnetic directions are suitable for magnetic polarity determination, and we define a total of eight paleomagnetic polarity zones straddling seven reversals (**Figure 7**). Integrated biostratigraphic data (Sutherland et al., 2019a and this work) help correlating these polarity zones with Chrons from C17n to C12r (**Figure 8**).

The presence of recovery gaps in the study succession likely produces errors due to the uncertainty in the position of the magnetostratigraphic boundaries that varies from a few thousand to less hundred thousand years.

A possible maximum uncertainty of less than 100 kyr is estimated for both the base of Chron C13n (247.72 ± 0.75 m; 37 kyr) and the base of Chron C13r (264.26 ± 0.75 m; ± 62 kyr). The latter is found within Core 30R (Figure 8) and the uncertainty is due to incomplete recovery (Table T1 in Sutherland et al., 2019a). A potential larger error (~± 94 kyr) should be taken into account when considering the base of Chron C15n (268.01 ± 1.5 m), which falls in the coring gap between Core 30R and Core 31R (Sutherland et al., 2019a) (**Table 2**). Finally, the position of the base of Chron C12r, lying between Core 20R and 21R, is at 237.260 ±3.75 m, the estimated uncertainty can cause a maximum error of ± 184 kyr.

All the possible errors related to the uncertainties in the position of magnetostratigraphic tie points as well as the errors associated with the paleontological sampling resolution (~15-30 kyrs on average) are reported in **Table 2**.

5. Discussion

5.1. Biochronological global comparison

The reliability of a bioevent is based on its synchronicity over wide areas (Raffi, 1999), the high repeatability among different workers, and its ranking and spacing compared with other biohorizons (Catanzariti et al., 1997). In the following discussion, we emphasize the limits and advantages of several main bioevents.

The **Top common and continuous of *Cribrocentrum reticulatum*** represents a virtually synchronous bioevent at low-middle latitudes. Our age estimate from the Tasman Sea (35.13 Ma) closely agrees with that reported for the Equatorial Indian Ocean (35.09) (Fioroni et al., 2015).

Instead, regarding the Top (T) of *C. reticulatum*, data from the GSSP section in Monte Cagnero (Hyland et al., 2009) provide an age of 35.12 Ma, similar to the age recorded at Site U1411 (Newsam, 2017) (**Figure 5**). These data are quite consistent with those from South Atlantic Sites 522 and 516, where the Top of this species has an age of 35.34 Ma and 35.29 Ma, respectively.

The **Top of *Discoaster barbadiensis*** occurs at 34.92 (±0.012) Myr and 400 kyr before the Top of *D. saipanensis* at Site U1509. Age estimates from low-middle latitude South and North Atlantic sites **(Figure 5)** are consistently younger than at U1509. Ages derived from the Equatorial Indian Ocean are virtually synchronous with U1509 (35.00 Ma).

The extinction of *D. barbadiensis* in the Equatorial Pacific Ocean (Site 1218) occurs 160 kyr after our age estimate at U1509, but the relative spacing with the Top of *D. saipanensis* seems to remain consistent. The Top of *D. barbadiensis* event is fairly reliable.

At Site U1509 the **Top of *Discoaster saipanensis*** occurs at 34.50 Ma (**Table 2**), which is consistent with the age derived from astronomical tuning (SM Table S1). There are possible minor discrepancies in age estimates from the Equatorial Pacific, Indian and Atlantic oceans. At Sites 1218 and 711, sedimentation rates are relatively low within Chron C13r (0.5 cm/kyr) and therefore possible small inconsistencies are likely the result of the summed effect of low sedimentation rates and/or poor magnetostratigraphic control, as is the case for Site 516 (Wei and Wise, 1989). Despite the above-mentioned sampling errors related to Chron boundaries placement, the two bioevents (tops of *D. barbadiensis* and *D. saipanensis*), are clearly spaced in time and in agreement with previous data.

The age estimate for the **Base common of *Clausicoccus subdistichus*** gr. at Site U1509 is 33.95 Ma. This result agrees with those reported from the Pacific and Atlantic Oceans (Toffanin et al., 2013; Newsam, 2017; **Figure 5**), giving further corroboration to the reliability of this datum for the middle-low latitudes.

At Site U1509 the ages of calcareous nannofossils for the upper part of the record were extrapolated considering the base Chron C12r and Chron C13n as tie-points, since the boundaries of Chron C12n are very poorly positioned though consistent with our age model (Sutherland et al.2019a). As a consequence, the precision of the ages assigned to calcareous nannofossil events is strictly dependent on the uncertainty in the position of the two magnetostratigraphic tie points (i.e. base Chron C12r and C13n). In the upper part of the study succession the base of Chron C12r lies in the core gap between Cores 27R and 28R, with a sampling gap of 7.5 m (233.51- 241.01 m) (**Table 2**) and a maximum age error of ±184 kyr using the mid-point between base and top sample.

The **Top of *Ericsonia formosa*** is a widely used biohorizon that benefits from easy recognition of the species, even in poorly preserved sediments (Wise, 1973). The disappearance of *E. formosa*, (32.94 Ma) at Site U1509 is consistent with age estimates from the Equatorial Pacific Ocean (32.90 Ma – Site 1218; 33.11 Ma– Hole U1333C) and for the Atlantic Ocean (32.82 Ma – Sites 522/523; 33.04 Ma Site 516; 33.20 Site U1411).

Overall, the extinction of this taxon appears globally synchronous and represents an excellent and consistent biohorizon (**Figure 5**).

The **Top of *Reticulofenestra umbilicus*** can be a problematic marker due to scattered occurrences towards the end of its upper range. Its extinction level records inconsistencies among workers and ocean basins as shown in **Figure 5**. The Top of *R. umbilicus* has been commonly applied as the early Oligocene marker (Martini, 1971; Okada and Bukry, 1980) based on its morphometrical differentiation. As suggested by Backman and Hermelin (1986), the criterion to distinguish *R. umbilicus* from other morphologically similar taxa is based on the size limit (>14 μm), and that criterion was used in this study. Age estimates for this bioevent from low-middle latitude sites are highly variable (between 31.10 Ma and 32.57 Ma) and the age derived at Site U1509 ranges from 29.98 to 32.18 Ma (accounting for an error of 2.2 Ma), considering both the uncertainty related to

the depth position of base Chron C12r and to that of base Chron C13n. Significant differences in the age of *R.umbilicus* among basins compared to the reference age estimate from the Pacific Ocean (31.98 Ma) could, at least in part, be related to ambiguous taxonomic/morphometric concepts of this species, since the size criterion (>14 µm) for *R. umbilicus* was not applied at all the investigated sites. In fact, the 14 µm size limit was not applicable at Site 1218 (Blaj et al., 2009) and not specified at Site 689/744 (Persico and Villa, 2004) and at Site 748 (Villa et al., 2008).

Notably, the shipboard data from Site U1509 placed this event at 177.07 ± 1.38 m, thus ~26 m above what observed in this work. We therefore recommend caution when using the Top of *R. umbilicus* since we consider the reliability of this datum to be relatively low.

5.2. Potential new biohorizons

The **Top common of *Clausicoccus subdistichus* gr.** is considered either diachronous in different regions (Backman, 1987) or not well defined because of the lack of sufficient data (Toffanin et al., 2013).

As reported by previous studies (e.g., Monechi, 1986a; Viganò et al., 2023), the Top of the acme interval of this species postdates the Top of *E. formosa*. Despite minor inconsistencies, our result from Site U1509 occurs 0.58 from the top of Zone CNO2 (considering the entire duration of CNO2 equals to 1) and is in good agreement with the position of this event at Site 756, supporting the idea that the Tc of *C. subdistichus* gr. could represent a useful bioevent, at least in some depositional settings such as mid-latitude marginal locations. The Tc of *Clausicoccus subdistichus* gr. recorded at Site U1509 has an age estimate of 32.17 Ma.

Despite the error in the age assignment of this bioevent, we suggest that the Tc of *C. subdistichus* gr. could be a useful datum for subdividing the long Zone CNO2 (duration ca. 900 kyr). Even if this event appears to be easy to detect at high-resolution, to date there is still a lack of data and more studies are required to assess its reproducibility at different latitudes and depositional settings.

The biostratigraphic significance of the **Top of *Isthmolithus recurvus*** is controversial (Backman, 1987).

A common opinion is that the Top of *I. recurvus* is consistent at middle to high latitudes, but this species is rare or absent at low latitudes, as confirmed by data from the Tanzanian Drilling Project (TDP) cores (TDP Sites 12 and 17) (Bown and Jones, 2006; Dunkley Jones et al., 2009). Results from the global compilation indicate that *I. recurvus* extinction occurred slightly earlier at middle latitudes (ca. 32.90 Ma) compared to high latitudes (32.46-32.68 Ma; Sites 689, 744 and 748). Based on this comparison, a short diachrony is confirmed between low-middle and high southern latitudes, as also suggested by Berggren et al. (1995).

Further investigations are required to assess the reliability of this bioevent, especially at low-middle latitudes. Our data corroborate the hypothesis that the abundance of *I. recurvus* strongly relied on latitudinal thermal gradients and on the ecological affinity of this taxon for high latitudes. This rationale is consistent with the distribution model found for this species, with low abundances per mm^2 at low-middle latitudes and higher abundances at higher latitudes (Monechi, 1986b). In the Southern Ocean this taxon is very abundant (up to 200 n/mm^2) (Persico and Villa, 2004; Villa et al., 2008) whereas data from Sites U1509 and 756 indicate similar patterns but with lower absolute abundances (up to 50 n/mm^2).

Lanternithus minutus has never been considered a reliable marker species due to its wide variance abundance across sites. However, the Bc and Tc of *L. minutus* appear to be interesting events, at least in specific depositional settings.

The acme interval of *L. minutus* is of short duration at Sites U1509 and 756 (Viganò et al., 2023), where it shows relatively low abundances (<5%). An acme interval of *L. minutus* was also reported from shelf areas of Central Paratethys (Ozsvárt et al., 2016; Nyerges et al., 2021), but with considerably higher quantitative abundances. However, it is undeniable that this species strongly relies on not yet fully understood local dynamics and specific conditions, as evidenced by the extremely rare abundance reported from the nearshore Cockspur Island and Pineora cores from North America (Self-Trail et al., 2019), or its absence in North Atlantic Site U1411 and North Pacific Site 1209 (Viganò et al., submitted). In the latter case, the absence of the fragile holococcolith *L. minutus* may be related to poor preservation.

In the South Atlantic Ocean (Site 1263; Bordiga et al., 2015) and in Tanzania (Sites 12, 17; Dunkley Jones et al., 2008), *L. minutus* displays similar and quite high abundances (up to 16% and 20%, respectively) but different abundance patterns and, in the latter case, a gradual decrease in abundance.

Among the other investigated taxa (*S. akropodus*, *S. predistentus* and *C. altus*), the Base of *S. predistentus* does not appear to be a useful biostratigraphic event due to rare and sporadic distribution of this species in the lower part of its stratigraphic range, as suggested by data available from Site 756 (Viganò et al., 2023). Instead, the Base of *S. akropodus* (**Figure 4**) is consistent with data reported from the Ninetyeast Ridge (Indian Ocean; Viganò et al., 2023), but needs to be further evaluated, especially considering that *S. akropodus* is extremely rare or even absent at some sites (e.g., Site U1411; Newsam, 2017).

We currently do not have sufficient data to evaluate the reliability of the Tc of *C. altus*, although the comparison of the abundance patterns of this taxon seems to suggest some spatial homogeneity and consistency between Site U1509 and Site 756 (Viganò et al., 2023). In our work, late Eocene forms of *Chiasmolithus* were ascribed to *C.* cf. *eoaltus* (**Figure 4**). Unfortunately, the lack of an unambiguous recognition of *C. eoaltus* hampers any biostratigraphic interpretations, especially considering that we did not observe the supposed gap between the Top of *C. eoaltus* and the base of *C. altus*. A further degree of complexity comes from the sporadic record of specimens of *C. eoaltus* between 184.50-231.31 m depth (early Oligocene), which has been interpreted as containing reworked sediment at Site U1509. More data are needed to sort this issue out, but the rarity and/or low preservation of this species at low-middle latitudes could have biased our data and confident correlation with high latitudes (Persico and Villa 2008; Fioroni et al., 2012) remains elusive.

5.3 Global application of biostratigraphic results

It has been known since the 1980s that diachroneity exists for some late Eocene - early Oligocene calcareous nannofossil biohorizons (e.g., Top of *D. saipanensis*; as discussed above in section 5.1) and that a low-middle latitude tropical biogeographic domain can be distinguished from a high latitude sub-Antarctic/Antarctic domain (Agnini et al., 2014 and references herein). Site U1509 is located in a key area of the western Pacific, one that may aid in the understanding this separation.

The modern tropical Pacific is subjected to strong easterly trade winds, whereas mid-high latitudes are subjected to westerlies. Collectively, these winds drive the South Pacific Gyre, whereby the East Australian

Current is the shallow return flow from the tropical western Pacific to the sub-tropical and sub-Antarctic Pacific (**Figure 2**) (Chiswell et al., 2015).

The Tasman Front, which lies just north of Site U1509, is the southern margin of a broad zone of easterly shallow current flow where the Eastern Australian Current returns tropical water (mixed with upwelled intermediate waters) to the mid-latitude Pacific (Ridgway & Dunn, 2003; Oke, Pilo, et al., 2019; Oke, Roughan, et al., 2019). The Subtropical Front is the southern extent to which tropical-sourced shallow waters can circulate, because strong circulation of the Antarctic Circumpolar Current (ACC) dominates shallow, intermediate and deep circulation further south (Bostock et al., 2015). Locations of the Tasman Front and Subtropical Front are strongly influenced by the location of land and shallow-ocean settings around New Zealand.

The ACC formed during the EOT when the southern end of South Tasman Rise (**Figure 2**) separated from Antarctica and allowed water from the southeast Indian Ocean to circulate into the Tasman Sea (Kennett et al., 1975). During the EOT, the paleolatitude of Sites U1509 and U1510 was ~44-45°S and 46-47°S, respectively (Dallanave et al., 2022), but Australia and New Zealand were also farther south. Site U1509 is located near to the South Tasman gateway and hence one might expect it to be one of the first locations in the global ocean to have been affected by ACC inception. However, we suggest Site U1509 remained beneath the southern extent of recirculating subtropical shallow waters, because New Zealand was farther south creating a barrier to easterly-flowing shallow ocean currents.

Paleontological results from Site U1509 are consistent with a low-middle latitude biogeographic domain during the EOT. In contrast, paleontological data from the Campbell Plateau at ~52°S (DSDP Site 277 and IODP Site U1553; EOT paleolatitude ~55 °S) belong to the late Eocene to early Oligocene Antarctic biogeographic domain (Kennett et al., 1975; Pascher et al, 2015; Röhl et al., 2020). The calcareous nannofossil low-middle latitude zonation of Agnini et al. (2014) was not applicable at Site U1553, while the Southern Ocean zonation of Fioroni et al (2012) fit a range of other observations during IODP Expedition 378 (Röhl et al., 2022).

Biostratigraphic and biochronological data from low-middle latitudes of the southern hemisphere precisely match those documented in the northern hemisphere, indicating that index species do not record either an amplification or a temporal lag between the two hemispheres. We might expect that opening of the South Tasman gateway and the onset of Antarctic glaciation affected the Tasman Sea first, resulting in a possible diachroneity of the first and last occurrences of calcareous nannofossil taxa, but our evidence is unable to resolve any difference in timing. We also do not find any correlation nor recognizable trends between paleoclimatic events and paleodepth estimates for our study sites. Therefore, we conclude that calcareous nannofossil bioevents discussed in paragraph 5.1 (i.e. the T of *E. formosa*, the Bc of *C. subdistichus*, the Tops of *D. barbadiensis* and *D. saipanensis* and the Tc of *C. reticulatum*) can be considered synchronous in the low-middle latitudes of the Pacific, Indian and Atlantic Oceans. However, relatively large inconsistencies remain for the Top of *R. umbilicus* and more studies are required to assess the reliability of the Tc of *C. subdistichus* gr. and *I. recurvus.*

6. Conclusions

We provide magnetostratigraphically calibrated age estimates for a series of biostratigraphic events from IODP Site U1509 (Tasman Sea), and compare them with those derived from Indian, Pacific, Atlantic and Southern Ocean sites. Our results lay the basis for evaluation of the synchronicity of calcareous nannofossil events during the late Eocene to early Oligocene and provide new insights on the potentiality of the Tc of *C. subdistichus* and the Tc of *I. recurvus* as new stratigraphic tools for correlation within Chron C12r (earliest Oligocene).

At Site U1509, age estimates for the Top of *E. formosa*, *D. saipanensis*, and *D. barbadiensis*, the Bc of *C. subdistichus* gr., and the Tc of *C. reticulatum* are consistent with those from the Equatorial Pacific, Indian and Atlantic Oceans. These bioevents are synchronous within the low-middle latitudes and between hemispheres. We find discrepancy in the extinction of *Reticulofenestra umbilicus* within Chron C12r. Possible explanations for this incongruity include: (i) bias based on the assumption of constant linear sedimentation during Chrons C13n and C12r and no local fault offset; (ii) the possibility that reworked specimens were used to place the event; or (iii) intrinsic errors due to the morphometric definition of this taxon. For these reasons, the Top of *R. umbilicus* should be used with caution, as also emphasized by Backman (1987) and Blaj et al. (2009). At all considered locations, the Bc of *C. subdistichus* gr. (33.90 Ma, GTS20) is the only calcareous nannofossil biohorizon useful to approximate the Eocene/Oligocene boundary (EOB). This event is preceded by the Top of *D. saipanensis* and the Top of *D. barbadiensis* (34.44 Ma and 34.76 Ma, respectively). The Bc of *C. subdistichus* gr. represents an alternative marker to approximate the position of the EOB, especially in the absence of planktonic foraminiferal biostratigraphy and/or oxygen isotopic data.

The comparison performed between Sites U1509 and U1510 and Sites 277 and U1553 interestingly points out that across and after the EOT Sites U1509 and U1510, with a paleolatitude estimation of ~44-45°S and 46-47°S, belonged to the Subtropical low-middle latitude domain implying a southern position for Subtropical Front (STF) with respect to the present-day. Theoretically, the position of the STF could have been established further south 46-47°S up to Campbell Plateau sites, which are instead located in the sub-Antarctic/Antarctic Southern Ocean domain.

We show that, during the late Eocene to early Oligocene, many of the discussed calcareous nannofossil events are characterized by latitudinal dualism. They are synchronous in different basins within the low-middle latitudes (i.e., in the Pacific – included Site U1509, Indian and Atlantic Oceans) - as for example the extinction of rosetta-shaped discoasters and *E. formosa* – but diachronous within the low-middle and high latitudes. This dualism is dependent upon recognition of a separate sub-Antarctic/Antarctic biogeographic domain influenced by the Antarctic Circumpolar Current.

Sites U1509 and U1510 had a paleolatitude of ~45°S and belonged to the Subtropical low-middle latitude (more global) domain, whereas Sites 277 and U1553 had a paleolatitude of ~55°S and belonged to the sub-Antarctic/Antarctic domain. The ancient equivalent of the Subtropical Front separated these two domains and was affected by paleogeographic positions of Tasmania, South Tasman Rise, and New Zealand; all of which were farther south during the EOT. Site U1509 is located close to this latitudinal ocean boundary (Subtropical Front) and in a part of the global ocean that was proximal to the South Tasman gateway (southern Tasman Sea), which had a key-role in driving climate evolution through the EOT. However, despite the close proximity of Site U1509 to the drivers of climate change, we can resolve no timing difference between Site U1509 and

other sites across much of the global ocean. We show a high degree of synchroneity of key calcareous nannofossil events in the middle-low latitude domain of both hemispheres, demonstrating important applications for precise biostratigraphic dating and correlation.

7. Acknowledgements

We thank the International Ocean Discovery Program (IODP) for providing samples and data used in this study. IODP is sponsored by the U.S. National Science Foundation (NSF) and participating countries under the management of Joint Oceanographic Institutions, Inc. ED was supported by the Deutsche Forschungsgemeinschaft (DFG project number 408178503). LA acknowledges support from Grant PID2019-105537RB-I00, funded by Ministerio de Ciencia e Innovación/ Agencia Estatal de Investigación / 10.13039/501100011033 and by "European Regional Development Funds, A way of making Europe".
Isabella Raffi and Davide Persico are deeply thanked for their constructive comments in the capacity of reviewers of A.V.' s PhD thesis during the evaluation process required by Italian law.

8. References

Agnini, C., Fornaciari, E., Raffi, I., Catanzariti, R., Pälike, H., Backman, J., Rio, D., 2014. Biozonation and biochronology of Paleogene calcareous nannofossils from low and middle latitudes. Newsletters on Stratigraphy 47, 131–181.

Agnini, C., Fornaciari, E., Raffi, I., Rio, D., Röhl, U., Westerhold, T., 2007. High-resolution nannofossil biochronology of middle Paleocene to early Eocene at ODP Site 1262: Implications for calcareous nannoplankton evolution. Marine Micropaleontology 64, 215–248.

Agnini, C., Monechi, S., Raffi, I., 2017. Calcareous nannofossil biostratigraphy: historical background and application in Cenozoic chronostratigraphy. Lethaia 50, 447–463.

Aubry, M.-P., 1992. Late Paleogene Calcareous Nannoplankton Evolution: A Tale of Climatic Deterioration. In: Prothero, D.R., Berggren, W.A., (Eds.), Eocene-Oligocene Climatic and Biotic Evolution, Princeton University Press, Princeton, NJ, 272-309.

Backman, J., 1987. Quantitative Calcareous Nannofossil Biochronology of Middle Eocene through Early Oligocene Sediment from DSDP Sites 522 and 523. Abhandlungen der Geologischen Bundesanstalt 39, 21–31.

Backman, J., Hermelin, J.O.R., 1986. Morphometry of the Eocene nannofossil Reticulofenestra umbilicus lineage and its biochronological consequences. Palaeogeography, Palaeoclimatology, Palaeoecology 57, 103–116.

Backman, J., Shackleton, N.J., 1983. Quantitative biochronology of Pliocene and early Pleistocene calcareous nannofossils from the Atlantic, Indian and Pacific oceans. Marine Micropaleontology 8, 141–170.

Berggren, W.A., 2001. International Time Scale. Encyclopedia of Life Sciences, https://doi.org/10.1038/npg.els.0001619.

Berggren, William A., Kent, D. V., Swisher, C.C., Aubry, Marie-Pierre, 1995. A Revised Cenozoic geochronology and chronostratigraphy. In: Berggren, W. A., Kent, D.V., Aubry, M.-P., Hardenbol, J. (Eds.), Geochronology, Time Scales, and Global Stratigraphic Correlation: A Unified Temporal Framework for an Historical Geology. Special publication - Society of Economic Paleontologists and Mineralogists, p. 129–212.

Blaj, T., Backman, J., Raffi, I., 2009. Late Eocene to Oligocene preservation history and biochronology of calcareous nannofossils from paleo-equatorial Pacific Ocean sediments. Rivista Italiana di Paleontologia e Stratigrafia 115, 67–85.

Bordiga, M., Henderiks, J., Tori, F., Monechi, S., Fenero, R., Legarda-Lisarri, A., Thomas, E., 2015. Microfossil evidence for trophic changes during the Eocene-Oligocene transition in the South Atlantic (ODP Site 1263, Walvis Ridge). Climate of the Past 11, 1249–1270.

Borrelli, C., Cramer, B.S., Katz, M.E., 2014. Bipolar Atlantic deepwater circulation in the middle-late Eocene: Effects of Southern Ocean gateway openings. Paleoceanography 29, 308–327.

Bostock, H. C., Hayward, B. W., Neil, H. L., Sabaa, A. T., & Scott, G. H., 2015. Changes in the position of the Subtropical Front south of New Zealand since the last glacial period. Paleoceanography 30, 824–844. https://doi.org/10.1002/2014PA002652.

Bowles, J. (2007). Coring-related deformation of Leg 208 sediments from Walvis Ridge: Implications for

667 paleomagnetic data. Physics of the Earth and Planetary Interiors, 161, 161–169.
668 https://doi.org/10.1016/j.pepi.2007.01.010
669 Bown, P.R., 1998. Calcareous nannofossil biostratigraphy. Chapman and Hall (Kluwer Academic Publishers),
670 London, UK, 314 p.
671 Bown, P.R., 2005. Paleogene calcareous nannofossils from the Kilwa and Lindi areas of coastal Tanzania
672 (Tanzania Drilling Project 2003-4). Journal of Nannoplankton Research 27, 21–95.
673 Bown, P.R., Dunkley Jones, T., 2006. New Palaeogene calcareous nannofossil taxa from coastal Tanzania:
674 Tanzania Drilling Project Sites 11 to 14. Journal of Nannoplankton Research 28, 17–34.
675 Bown, P.R., Dunkley Jones, T., 2012. Calcareous nannofossils from the Paleogene equatorial Pacific (IODP
676 Expedition 320 Sites U1331-1334). Journal of Nannoplankton Research 32, 3–51.
677 Bown, P.R., Newsam, C., 2017. Calcareous nannofossils from the Eocene North Atlantic Ocean (IODP
678 Expedition 342 Sites U1403–1411). Journal of Nannoplankton Research 37, 25–60.
679 Bown, P.R., Young, J.R., 1998. Techniques. In: Bown, P.R. (Ed.), Calcareous Nannofossil Biostratigraphy.
680 Kluwer Academic Publishers, London, p. 16–28.
681 Bukry, D., 1973. Low-latitude coccolith biostratigraphic zonation. Initial Reports of the Deep Sea Drilling
682 Project, 15 685–703.
683 Bukry, D., 1978. Biostratigraphy of Cenozoic marine sediment by calcareous nannofossils. Micropaleontology
684 24, 44–60.
685 Cande, S.C., Kent, D.V., 1992. A new geomagnetic polarity timescale for the Late Cretaceous and Cenozoic.
686 Journal of Geophysical Research 97, 13917–13951.
687 Cande, S.C., Stock, J.M., 2004. Cenozoic Reconstructions of the Australia-New Zealand-South Pacific Sector
688 of Antarctica. In The Cenozoic Southern Ocean: Tectonics, Sedimentation, and Climate Change
689 Between Australia and Antarctica (eds. Exon, N. F., Kennett, J. P. & Malone, M. J.) vol. 151 5–17.
690 Catanzariti, R., Rio, D., Martelli, L., 1997. Late Eocene to Oligocene calcareous nannofossil Biostratigraphy
691 in Northern Apennines: the Ranzano sandstone. Memorie di Scienze Geologiche 49, 207–253.
692 Chiswell, S.M., Bostock, H.C., Sutton, P.J.H., Williams, M.J., 2015. Physical oceanography of the deep seas
693 around New Zealand: A review. New Zealand Journal of Marine and Freshwater Research 49, 286–317.
694 Coccioni, Rodolfo, Monaco, P., Monechi, S., Nocchi, M., Parisi, G., 1988. Biostratigraphy of the Eocene-
695 Oligocene bonudary at Massignano (Ancona, Italy). In: Premoli Silva, I., Coccioni, R., Montanari, A.
696 (Eds.), The Eocene–Oligocene Boundary in the March-Umbria Basin (Italy). Fratelli Anniballi, Ancona,
697 p. 81–96.
698 Constable, C., Tauxe, L., 1990. The bootstrap for magnetic susceptibility tensors. Journal of Geophysical
699 Research, 95(B6), 8383–8395, https://doi.org/10.1029/JB095iB06p08383.
700 Coxall, H.K., Wilson, P.A., Pälike, H., Lear, C.H., Backman, J., 2005. Rapid stepwise onset of Antarctic
701 glaciation and deeper calcite compensation in the Pacific Ocean. Nature 433, 53–7.
702 Coxall, H. K., & Pearson, P. N., 2007. The Eocene-Oligocene Transition. In: M. Williams, A. M. Haywood,
703 J. Gregory, & D. N. Schmidt (Eds.), Deep-Time Perspectives on Climate Change: Marrying the Signal
704 from Computer Models and Biological Proxies, Micropaleontology Society Special Publication London:
705 Geological Society, p. 351–387).

706 Crouch, E. M., Clowes, C. D., Raine, J. I., Alegret, L., Cramwinckel, M. J., & Sutherland, R., 2022. Latest
707 cretaceous and paleocene biostratigraphy and paleogeography of northern zealandia, IODP site U1509,
708 New Caledonia Trough, southwest pacific. New Zealand Journal of Geology and Geophysics,
709 https://doi:10.1080/00288306.2022.2090386.
710 Dallanave, E., Chang, L., 2020. Early Eocene to early Miocene magnetostratigraphic framework for IODP
711 Expedition 371 (Tasman Frontier Subduction Initiation and Paleogene Climate). Newsletters on
712 Stratigraphy 53(4), 365–387, https://doi.org/10.1127/nos/2019/0556.
713 Dallanave, E., Kirscher, U., 2020. Testing the reliability of sedimentary paleomagnetic datasets for
714 paleogeographic reconstructions. Frontiers in Earth Science, Geomagnetism and Paleomagnetism 8,
715 592277, 1–16. https://doi.org/10.3389/feart.2020.592277.
716 Dallanave, E., Sutherland, R., Dickens, G.R., Chang, L., Tema, E., Alegret, L., Agnini, C., Westerhold, T.,
717 Newsam, C., Lam, A.R., Stratford, W.R., Collot, J., Etienne, S.J.G., Von Dobeneck, T., 2022. Absolute
718 Paleolatitude of Northern Zealandia from the Middle Eocene to the Early Miocene. J. Geophys. Res.
719 Solid Earth 127, 1–19. https://doi.org/10.1029/2022JB024736
720 Diekmann, B., Kuhn, G., Gersonde, R., Mackensen, A., 2004. Middle Eocene to early Miocene environmental
721 changes in the sub-Antarctic Southern Ocean: Evidence from biogenic and terrigenous depositional
722 patterns at ODP Site 1090. Global and Planetary Change 40, 295–313.
723 Diester-Haass, L., Zahn, R., 1996. Eocene-Oligocene transition in the Southern Ocean: History of water mass
724 circulation and biological productivity. Geology 24, 163–166.
725 Dunkley Jones, T., Bown, P.R., Pearson, P.N., 2009. Exceptionally well preserved upper Eocene to lower
726 Oligocene calcareous nannofossils (Prymnesiophyceae) from the Pande Formation (Kilwa Group),
727 Tanzania. Journal of Systematic Palaeontology 7, 359–411.
728 Dunkley Jones, T., Bown, P.R., Pearson, P.N., Wade, B.S., Coxall, H.K., Lear, C.H., 2008. Major shifts in
729 calcareous phytoplankton assemblages through the Eocene-Oligocene transition of Tanzania and their
730 implications for low-latitude primary production. Paleoceanography 23, 1–14.
731 Etienne, S., Collot, J., Sutherland, R., Patriat, M., Bache, F., Rouillard, P., Juan, C., 2018. Deepwater
732 sedimentation and Cenozoic deformation in the southern New Caledonia Trough (northern Zealandia,
733 SW Pacific). Marine and Petroleum Geology 92, 764-779. https://doi:10.1016/j.marpetgeo.2017.12.007.
734 Fioroni, C., Villa, G., Persico, D., Wise, S.W., Pea, L., 2012. Revised middle Eocene-upper Oligocene
735 calcareous nannofossil biozonation for the Southern Ocean. Revue de Micropaleontologie 55, 53-70.
736 Fioroni, C., Villa, G., Persico, D., Wise, S.W., and Pea, L., 2012. Revised middle Eocene-upper Oligocene
737 calcareous nannofossil biozonation for the Southern Ocean. Revue de Micropaléontologie, 55(2), 53–
738 70. https://doi.org/10.1016/j.revmic.2012.03.001.
739 Fioroni, C., Villa, G., Persico, D., Jovane, L., 2015. Middle Eocene-Lower Oligocene calcareous nannofossil
740 biostratigraphy and paleoceanographic implications from Site 711 (equatorial Indian Ocean). Marine
741 Micropaleontology 118, 50–62.
742 Fisher, R., 1953. Dispersion on a sphere. Proceedings of the Royal Society of London, A217, 295–305.
743 Fisher, R., 1957. The underworld of probability. Sankhyā: The Indian Journal of Statistics (1933-1960) 18
744 (3/4), 201–210.

Gradstein, F.M., Ogg, J.G., Schmitz, M.D., Ogg, G.M., 2020. The Geologic Time Scale 2020. Elsevier, Amsterdam, Netherlands, v.1-2, 1357p.

Hallam, A., Hancock, J.M., LaBreque, J.L., Lowrie, W., Channell, J.E.T., 1985. Jurassic to Palaeogene magnetostratigraphy. In: Snelling, N.J. (Eds.), The Chronology of the Geological Record. Geological Society of London 10, p. 118–140.

Hyland, E., Murphy, B.H., Varela, P., Marks, K., Colwell, L., Tori, F., Monechi, S., Cleaveland, L., Brinkhuis, H., Van Mourik, C.A., Coccioni, R., Bice, D.M., Montanari, Alessandro, 2009. Integrated stratigraphic and astrochronologic calibration of the Eocene-Oligocene transition in the Monte Cagnero section (northeastern Apennines, Italy): A potential parastratotype for the Massignano global stratotype section and point (GSSP). In: Koeberl, C., Montanari, A. (Eds.), The Late Eocene Eart Hothouse, Icehouse, and Impacts. The Geological Society of America Special Paper 452, p. 303–322.

Hsü, K.J., LaBrecque, J., Pisciotto, K.A., 1984. Site 523. Initial reports DSDP, Leg 73 271–321.

Hutchinson, D. K., Coxall, H. K., Lunt, D. J., Steinthorsdottir, M., de Boer, A. M., Baatsen, M., von der Heydt, A., Huber, M., Kennedy-Asser, A. T., Kunzmann, L., Ladant, J.-B., Lear, C. H., Moraweck, K., Pearson, P. N., Piga, E., Pound, M. J., Salzmann, U., Scher, H. D., Sijp, W. P., Śliwińska, K. K., Wilson, P. A., and Zhang, Z., 2021. The Eocene–Oligocene transition: a review of marine and terrestrial proxy data, models and model–data comparisons, Climate of the Past 17, 269–315, https://doi.org/10.5194/cp-17-269-2021, 2021 .

Jelínek, V., 1977. The Statistical Theory of Measuring Anisotropy of Magnetic Susceptibility of Rocks and its Application. Brno, Czech Republic: Geofyzika Brno, p.88.

Jelinek, V., 1981. Characterization of the magnetic fabric of rocks. Tectonophysics 79, T63–T67.

Jovane, L., Savian, J.F., Coccioni, R., Frontalini, F., Bancala, G., Catanzariti, R., Luciani, V., Bohaty, S.M., Wilson, P.A., Florindo, F., 2015. Integrated magnetobiostratigraphy of the middle Eocene – lower Oligocene interval from the Monte Cagnero section , central Italy Ocean and Earth Science , University of Southampton , National Oceanography Centre. In: Jovane, L., Herrero-Bervera, E., Hinnov, L.A., Housen, B.A. (Eds.), Magnetic Methods and the Timing of Geological Processes. Geological Society, London, Special Publications, p. 79–95.

Kennett, J.P., Burns, R.E., Andrews, J.E., Churkin Jr. M., Davies, T.A. Dumitrica, P., Edwards, A.R., Galehouse, J.S., Packham, G.H., Van Der Lingen G.J., 1972. Australian-antarctic continental drift, palaeocirculation changes and oligocene deep-sea erosion Nature Physical Science 239, 51-55.

Kennett, J.P., Houtz, R.E., Andrews, P.B., Edwards, A.R., Gostin, V.A., Hajos, M., Hampton, M., Jenkins, D.G., Margolis, S.V., Ovenshine, A.T., Perch-Nielsen, K.,, 1975. Cenozoic paleoceanography in the southwest Pacific Ocean, Antarctic glaciation and the development of the circum-Antarctic current. In: Kennett JP et al. (Eds.), Init Rep DSDP 21.,U.S. Govt Printing Office, Washington, p. 1155–1169.

Kennett, J. P., 1977. Cenozoic evolution of Antarctic glaciation, the circum-Antarctic Ocean, and their impact on global paleoceanography. Journal of Geophysical Research 82 (27), 3843-3860, https://doi:10.1029/jc082i027p03843.

Kirschvink, J. L., 1980. The least-squares line and plane and the analysis of palaeomagnetic data. Geophysical Journal of the Royal Astronomical Society 62(3), 699–718, https://doi.org/10.1111/j.1365-

246X.1980.tb02601.x.

Lear, C.H., Rosenthal, Y., Coxall, H.K., Wilson, P.A., 2004. Late Eocene to early Miocene ice sheet dynamics and the global carbon cycle. Paleoceanography 19, 1–11.

Li, Y.-X., Wang, S., Fu, S., Jiao, W., 2014. Recognizing the threshold magnetic anisotropy for inclination shallowing: Implications for correcting inclination errors of sedimentary rocks. Frontiers in Earth Science, 2 , 1–17, https://doi.org/10.3389/feart.2014.00008.

Madile, M., Monechi, S., 1991. Late Eocene to early Oligocene calcareous nannofossil assemblages from Sites 699 and 703, subantarctic South Atlantic Ocean. Proceedings of the Ocean Drilling Program, Scientific Results, 114, 179–192.

Marino, M., Flores, J.A., 2002. Middle Eocene to early Oligocene calcareous nannofossil stratigraphy at Leg 177 Site 1090. Marine Micropaleontology 45, 383–398.

Martini, E., 1971. Standard Tertiary and Quaternary calcareous nannoplankton zonation. In: Farinacci, A. (Ed.), Proceedings of the 2nd International Conference on Planktonic Microfossils. Edizioni Tecnoscienza, Rome, p. 739–785.

McFadden, P.L., Reid, A.B., 1982. Analysis of palaeomagnetic inclination data. Geophysical Journal of the Royal Astronomical Society, 69, 307–319.Monechi, S., 1986a. Biostratigraphy of Fuente Caldera Section by Means of Calcareous Nannofossils. Developments in Palaeontology and Stratigraphy 9, 65-69.

Monechi, S., 1986. Calcareous nannofossil events around the Eocene-Oligocene boundary in the Umbrian Apennines (Italy). Palaeogeography, Palaeoclimatology, Palaeoecology 57, 61–69.

Mortimer, N., Campbell, H. J., Tulloch, A. J., King, P. R., Stagpoole, V. M., Wood, R. A., et al. (2017). Zealandia: Earth's hidden continent. Geological Society of America Today, 27, 1–8. https://doi.org/10.1130/GSATG321A.1.

Mullender, T.A., Frederichs, T., Hilgenfeldt, C., de Groot, L. V., Fabian, K., Dekkers, M.J., 2016. Automated paleomagnetic and rock magnetic data acquisition with an in-line horizontal “‘2G”’ system Tom. Geochemistry, Geophysics, Geosystems 17, 3546–3559. https://doi.org/10.1002/ 2016GC006436.

Müller, R.D., Cannon, J., Qin, X., Watson, R.J., Gurnis, M., Williams, S., Pfaffelmoser, T., Seton, M., Russell, S.H.J., Zahirovic, S., 2018. GPlates: Building a virtual earth through deep time. Geochemistry, Geophys. Geosystems 19, 2243–2261, https://doi.org/10.1029/2018GC007584.

Newsam, C., 2017. Calcareous nannoplankton evolution and the Paleogene greenhouse to icehouse climate-mode transition. Ph.D. Thesis, University College of London, London, Great Britain, 224p.

Norris, R.D., Wilson, P.A., Blum, P., Fehr, A., Agnini, C., Bornemann, A., Boulila, S., Bown, P.R., Cournede, C., Friedrich, O., Ghosh, A.K., Hollis, C.J., Hull, P.M., Jo, K., Junium, C.K., Kaneko, M., Liebrand, D., Lippert, P.C., Liu, Z., Matsui, H., Moriya, K., Nishi, H., Opdyke, B.N., Penman, D.E., Romans, B.W., Scher, H.D., Sexton, P., Takagi, H., Turner, S.K., Whiteside, J.H., Yamaguchi, T., Yamamoto, Y., 2014. Site U1411. Proceedings of the Integrated Ocean Drilling Program 342, http://publications.iodp.org/proceedings/342/112/112_.htm.

Nyerges, A. Kocsis, Á. T., Pálfy, J., 2021. Changes in calcareous nannoplankton assemblages around the Eocene-Oligocene climate transition in the Hungarian Palaeogene Basin (Central Paratethys), Historical

Biology 33(9), 1443-1456, https://10.1080/08912963.2019.1705295.
Okada, H., Bukry, D., 1980. Supplementary modification and introduction of code numbers to the low-latitude coccolith biostratigraphic zonation. Marine Micropaleontology 5, 321–325.
Oke, P. R., Pilo, G. S., Ridgway, K., Kiss, A., Rykova, T., 2019. A search for the Tasman Front. Journal of Marine Systems, 199, 103217.
Oke, P.R., Roughan, M., Cetina-Heredia, P., Pilo, G.S., Ridgway, K.R., Rykova, T., Archer, M.R., Coleman, R.C., Kerry, C.G., Rocha, C., Schaeffer, A., Vitarelli, E., 2019. Revisiting the circulation of the East Australian Current: Its path, separation, and eddy field. Progress in Oceanography 176, 102139.
Ozsvárt, P., Kocsis, L., Nyerges, A., Győri, O., Pálfy, J., 2016. The Eocene-Oligocene climate transition in the Central Paratethys. Palaeogeography, Palaeoclimatology, Palaeoecology 459, 471–487.
Pascher, K. M., Hollis, C. J., Bohaty, S. M., Cortese, G., McKay, R. M., Seebeck, H., Suzuki N., Chiba, K., 2015. Expansion and diversification of high-latitude radiolarian assemblages in the late eocene linked to a cooling event in the southwest pacific. Climate of the Past 11(12), 1599-1620. https://doi:10.5194/cp-11-1599-2015.
Persico, D., Fioroni, C., Villa, G., 2012. A refined calcareous nannofossil biostratigraphy for the middle Eocene-early Oligocene Southern Ocean ODP sites. Palaeogeography, Palaeoclimatology, Palaeoecology 335–336, 12–23.
Persico, D., Villa, G., 2004. Eocene-Oligocene calcareous nannofossils from Maud Rise and Kerguelen Plateau (Antarctica): Paleoecological and paleoceanographic implications. Marine Micropaleontology 52, 153–179.
Persico, D., Villa G., 2008. A new Eocene Chiasmolithus species: hypothetical reconstruction of its phyletic lineage. Journal of Nannoplankton Research 30, 23-33.
Premoli Silva, I., Orlando, M., Monechi, S., Madile, M., Napoleone, G., Ripepe, M., 1988. Calcareous plankton biostratigraphy and magnetostratigraphy at the Eocene-Oligocene transition in the Gubbio area. International Subcommission on Paleogene Stratigraphy, Eocene/Oligocene Meeting, Spec. Publ., II 6, 137–161.
Pusz, A.E., Thunell, R.C., Miller, K.G., 2011. Deep water temperature, carbonate ion, and ice volume changes across the Eocene-Oligocene climate transition. Paleoceanography 26, 1–15.
Raffi, I., 1999. Precision and accuracy of nannofossil biostratigraphic correlation. Philosophical Transactions of the Royal Society A: Mathematical, Physical and Engineering Sciences 357, 1975–1993.
Raffi, I., Agnini, C., Backman, J., Catanzariti, R., Pälike, H., 2016. A Cenozoic calcareous nannofossil biozonation from low and middle latitudes: A synthesis. Journal of Nannoplankton Research 36, 121–132.
Ridgway, K., Dunn, J., 2003. Mesoscale structure of the mean East Australian Current System and its relationship with topography. Progress in Oceanography 56(2), 189–222.
Röhl, U., Thomas, D.J., Childress, L.B., Anagnostou, E., Ausín, B., Borba Dias, B., Boscolo-Galazzo, F., Brzelinski, S., Dunlea, A.G., George, S.C., Haynes, L.L., Hendy, I.L., Jones, H.L., Khanolkar, S.S., Kitch, G.D., Lee, H., Raffi, I., Reis, A.J., Sheward, R.M., Sibert, E., Tanaka, E., Wilkens, R., Yasukawa, K., Yuan, W., Zhang, Q., Zhang, Y., Drury, A.J., and Hollis, C.J., 2022. Expedition 378 summary. In

Röhl, U., Thomas, D.J., Childress, L.B., and the Expedition 378 Scientists, South Pacific Paleogene Climate. Proceedings of the International Ocean Discovery Program, 378: College Station, TX (International Ocean Discovery Program). https://doi.org/10.14379/iodp.proc.378.101.2022.

Self-Trail, J.M., Parker, M., Haynes, J.T., Schultz, A.P., Huddlestun, P.F., 2019. Geology and biostratigraphy of the Upper Floridan aquifer in the greater Savannah region, Georgia and South Carolina. Stratigraphy 16, 41–62.

Shafik, S., 1981. Nannofossil biostratigraphy of the Hankenina (foraminiferal) interval in the upper Eocene of southern Australia. BMR Journal of Australian Geology & Geophysics 6, 108–116.

Sijp, W.P., England,M.H., Toggweiler, J.R., 2009. Effect of ocean gateway changes under greenhouse warmth. Journal of Climate 22 (24), 6639–6652.

Stradner, H., 1962. Über neue und wenig bekannte Nannofossilien aus Kreide und Alttertiär. Sonderabdruck aus den Verhandlungen der Geologischen Bundesanstalt 2, 363–377.

Sutherland, R., Collot, J., Bache, F., Henrys, S., Barker, D., Browne, G.H., Lawrence, M.J.F., Morgans, H., Hollis, C.J., Clowes, C., Mortimer, N. ,Rouillard, P., Gurnis, M., Etienne, S., Stratford W., 2017. Widespread compression associated with Eocene Tonga-Kermadec subduction initiation Geology 45, 355-358.

Sutherland, R., Dickens, G.R., Blum, P., Agnini, C., Alegret, L., Bhattacharya, J., Bordenave, A., Chang, Li., Collot, J., Cramwinckel, M.J., Dallanave, E., Drake, M.K., Etienne, S.J.G., Giorgioni, M., Gurnis, M., Harper, D.T., Huang, H., Keller, A.L., Lam, A.R., Li, H., Matsui, H., Morgans, H.E.G., Newsam, C., Park, Y.H., Pascher, K.M., Pekar, S.F., Penman, D.E., Saito, S., Stratford, W.R., Westerhold, T., Zhou, X., 2018. Expedition 371 Preliminary Report: Tasman Frontier Subduction Initiation and Paleogene Climate. International Ocean Discovery Program. https://doi.org/10.14379/iodp.pr.371.2018.

Sutherland, R., Dickens, G.R., Blum, P., Agnini, C., Alegret, L., Bhattacharya, J., Bordenave, A., Chang, Li., Collot, J., Cramwinckel, M.J., Dallanave, E., Drake, M.K., Etienne, S.J.G., Giorgioni, M., Gurnis, M., Harper, D.T., Huang, H., Keller, A.L., Lam, A.R., Li, H., Matsui, H., Morgans, H.E.G., Newsam, C., Park, Y.H., Pascher, K.M., Pekar, S.F., Penman, D.E., Saito, S., Stratford, W.R., Westerhold, T., Zhou, X., 2019a. Site U1509. Proceedings of the International Ocean Discovery Program Volume 371, https://doi.org/10.14379/iodp.proc.371.106.2019

Sutherland, R., Dickens, G.R., Blum, P., Agnini, C., Alegret, L., Bhattacharya, J., Bordenave, A., Chang, Li., Collot, J., Cramwinckel, M.J., Dallanave, E., Drake, M.K., Etienne, S.J.G., Giorgioni, M., Gurnis, M., Harper, D.T., Huang, H., Keller, A.L., Lam, A.R., Li, H., Matsui, H., Morgans, H.E.G., Newsam, C., Park, Y.H., Pascher, K.M., Pekar, S.F., Penman, D.E., Saito, S., Stratford, W.R., Westerhold, T., Zhou, X., 2019b. Expedition 371 methods. Proceedings of the International Ocean Discovery Program Volume 371, https://doi.org/10.14379/iodp.proc.371.102.2019.

Sutherland, R., Dos Santos, Z., Agnini, C., Alegret, L., Lam, A.R., Westerhold, T., Drake, M.K., Harper, D.T., Dallanave, E., Newsam, C., Cramwinckel, M.J., Dickens, G.R., Collot, J., Etienne, S.J.G., Bordenave, A., Stratford, W.R., Zhou, X., Li, H., Asatryan, G., 2022. Neogene Mass Accumulation Rate of Carbonate Sediment Across Northern Zealandia, Tasman Sea, Southwest Pacific. Paleoceanography and Paleoclimatology 37, 1–22.

Tetley, M.G., Williams, S.E., Gurnis, M., Flament, N., Müller, R.D., 2019. Constraining Absolute Plate Motions Since the Triassic. J. Geophys. Res. Solid Earth 124, 7231-7258. https://doi.org/10.1029/2019JB017442Toffanin, F., Agnini, C., Rio, D., Acton, G., Westerhold, T., 2013. Middle eocene to early oligocene calcareous nannofossil biostratigraphy at IODP site U1333 (Equatorial Pacific). Micropaleontology 59, 69–82.

Villa, G., Fioroni, C., Pea, L., Bohaty, S.M., Persico, D., 2008. Middle Eocene-late Oligocene climate variability: Calcareous nannofossil response at Kerguelen Plateau, Site 748. Marine Micropaleontology 69, 173–192.

Viganò, A., Coxall, H.K., Holmström, M., Vinco, M., Lear, C.H., Agnini, C., 2023. Calcareous nannofossils across the Eocene-Oligocene transition at Site 756 (Ninetyeast Ridge, Indian Ocean): implications for biostratigraphy and paleoceanographic clues. Newsletters on Stratigraphy 56 (2), 187-223.

Wei, W., 1991. Middle Eocene-lower Miocene calcareous nannofossil magnetobiochronology of ODP Holes 699A and 703A in the subantarctic South Atlantic. Marine Micropaleontology 18, 143–165.

Wei, W., Wise, S.W., 1989. Paleogene calcareous nannofossil magnetobiochronology: Results from South Atlantic DSDP Site 516. Marine Micropaleontology 14, 119–152.

Wei, W., Wise, S.W., 1990. Biogeographic gradients of middle Eocene-Oligocene calcareous nannoplankton in the South Atlantic Ocean. Palaeogeography, Palaeoclimatology, Palaeoecology 79, 29–61.

Wise, S.W., 1973. Calcareous nannofossils from cores recovered during Leg 18, Deep Sea Drilling Project: biostratigraphy and observations on diagenesis. In: Kulm, L.D., Huene, R. von, Et, A. (Eds.), Initial Reports of the Deep Sea Drilling Project, 18. U.S. Government Printing Office, Washington, D.C., p. 569–515.

Wise, S.W., 1983. Mesozoic and Cenozoic calcareous nannofossils recovered by Deep Sea Drilling Project Leg 71 in the Falkland Plateau region, southwest Atlantic Ocean. Init. Repts. DSDP, 71 481–550.

Wright, N.M., Scher, H.D., Seton, M., Huck, C.E., Duggan, B.D., 2018. No Change in Southern Ocean Circulation in the Indian Ocean From the Eocene Through Late Oligocene. Paleoceanography and Paleoclimatology 33, 152–167.

Zachos, J.C., Quinn, T.M., Salamy, K.A., 1996. High-resolution (10^4 years) deep-sea foraminiferal stable isotope records of the Eocene-Oligocene climate transition. Paleoceanography 11, 251–266.

Zachos, J. C., Pagani, M., Sloan, L., Thomas, E., & Billups, K., 2001. Trends, Global Rhythms, and Aberrations in Global Climate 65 Ma to Present. Science, 292, 686–693. https://doi.org/10.1126/science.1059412.

Zachos, J.C., Dickens, G.R., Zeebe, R.E., 2008. An early Cenozoic perspective on greenhouse warming and carbon-cycle dynamics. Nature 451, 279–283.

Zijderveld, J. D. A., 1967. A.C. demagnetization of rocks: Analysis of results. In: D. W. Collinson, K. M. Creer, and S. K. Runcorn (Eds.), Methods in Paleomagnetism New York: Elsevier, p. 254–286.

9. Figure Captions

Figure 1. Paleo map reconstruction centered on the E-O transition (~34 Ma) showing the location of IODP Site U1509 (solid red star, IODP Exp. 371) and other low-middle latitude sites (IODP Site U1411, IODP Exp. 342; Sites 522/523, DSDP Leg. 73; 516, DSDP Leg. 72; Site 711, ODP Leg. 115; Site 756, ODP Leg. 121; Site 1218, ODP Leg 199; Site 1333, IODP Exp. 320; references are reported in the main text) and high-latitude sites used herein for comparison (Site 1090, ODP Leg. 177; Site 744, ODP Leg. 119; Site 748, ODP Leg. Site 120; 689, ODP Leg. 113; references in the text). Purple dot = Pacific Ocean; green dot = Atlantic Ocean; light blue dot: Indian Ocean. Paleogeographic map was generated with GPlates (Müller et al., 2018) using the rotation parameters of Tetley et al. (2019), with the global plate position fixed with respect to the Earth's spin axis through linear interpolation of the paleomagnetic poles presented in Dallanave et al. (2022).

Figure 2. Map of Tasman Sea bathymetry (color shading, ETOPO data set, https://www.ngdc.noaa.gov/mgg/global/) and surface ocean currents (dashed red arrows) after Ridgway and Dunn (2003). White circles are Deep Sea Drilling Program (DSDP)/International Ocean Discovery Program (IODP) drill sites and white stars are IODP Expedition 371 sites.

Figure 3. Integrated bio-magnetochronostratigraphy of the study interval. Chronostratigraphy is after GTS20. Calcareous nannofossil schemes: CP zones, Okada and Bukry, 1980; NP Zones, Martini, 1971; CNE and CNO Zones, Agnini et al., 2014. Biochronology after Agnini et al. (2014) recalibrated to GTS20.

Figure 4. Semi-quantitative (n/mm^2, in solid grey area) and relative (%, black line and dotted red line) abundance patterns of biostratigraphically useful calcareous nannofossil taxa from Site U1509, compared along with depth (CSF-A, m), magnetostratigraphy, calcareous nannofossil (CN) (Martini, 1971; Okada & Bukry, 1980; Agnini et al., 2014) and planktonic foraminiferal (PF) (Wade et al., 2011) biozonations, and chronostratigraphy. The dashed horizontal line specifies the extrapolated position of the EOB based on LSR. The position of the bioevents is indicated as B = Base, Bc= Base continuous and common, T = Top, Tc= Top continuous and common.

Figure 5. Correlation of the main biostratigraphic events based on magnetostratigraphy as recognized in different low-middle and high latitude sites. Age estimates were calibrated to GTS20 of Gradstein et al. (2020). Data are from Tasman Sea (Site U1509, this study), Equatorial Pacific Ocean (Site 1218, Blaj et al., 2009), Site U1333, Toffanin et al., 2013), Equatorial Indian Ocean (Site 711, Fioroni et al., 2015), South Atlantic (Sites 522, 523, Backman, 1987; Site 516 from Wei and Wise, 1989), North Atlantic (Site U1411, Newsam, 2017) and Southern Ocean (Site 1090, Marino and Flores, 2002; Site 689 and Site 744, Persico and Villa, 2004; Site 748, Villa et al., 2008). The size limit of >14 µm for *R. umbilicus* was adopted in this work (Site U1509) and at Sites 711, 522, 523; it was not specified at Site 689,744 and Site 748 and not applicable at Site 1218.

Figure 6. Anisotropy of magnetic susceptibility (AMS) results. A) Equal area projection of the AMS tensor axes of all samples. B) Results of 1000 averaged bootstrapped datasets, with cumulative distribution of the eigenvalues associated to the AMS eigenvectors.

Figure 7. Representative vector end-points demagnetization diagrams and average inclination. A) Example of diagram with a up-pointing (i.e., normal paleomagnetic polarity) characteristic remanence magnetization (ChRM); open (closed) symbols are projection onto the vertical (horizontal) plane; demagnetization steps are

in mT; red symbols are the vector end-points interpolated for the ChRM with principal component analysis, with the resulted ChRM indicated by the blue dashed line. B) Example of down-pointing (i.e., reversed polarity) ChRM diagram, with symbols as in panel (A). C) Example of diagram with ChRM vector end-points averaged by Fisher (1957) statistics. D) Average inclinations of the down- and up-pointing directions determined as explained in the main text, as well as of the whole dataset combined in a common down-pointing mode.

Figure 8. Magnetostratigraphic results. From left to right: studied record with indication of depth, core number, recovery, and lithology; results from anisotropy of magnetic susceptibility (AMS) analysis: absolute susceptibility, corrected anisotropy degree "Pj" of Jelinek (1981), inclination of the minor k3 axis of the AMS (90°= vertical); results of the natural remanent magnetization (NRM) analysis: ChRM inc.= characteristic remanent magnetization inclination, with the discrete samples results from this work indicated by the yellow diamonds, while the light blue dots are single measurement points of the archive half after 20 mT cleaning measured onboard (Sutherland et al., 2019-U1509 chapter); magnetic polarity interpretation (white= reversed polarity, black= normal polarity, gray= undetermined) and correlation with the geomagnetic polarity time scale (Ogg, 2020).

10.Table Captions

Table 1. Location of the study site (IODP Site U1509) and other sites used for comparison. Location, geographic coordinates, current water depth (m), paleodepth (m) and references are reported for each IODP, ODP and DSDP site. Paleodepths are after Lear et al. (2004), Coxall et al. (2005) and Borrelli et al. (2014) for Site 1218, Zachos et al. (1996) for Site 522 and Hsü et al. (1984) for Site 523, Pusz et al. 2011 for Site 1090, Diester-Haass and Zahn (1996) and Borrelli et al. (2014) for Site 689, Wright et al. (2018) for Site 744 and 748.

Table 2. Positions and age estimates of selected biohorizons at IODP Site U1509 and EOIS ($\delta^{18}O$ bulk isotopes) based on magnetostratigraphic tie-points (in bold). Note: B = Base, Bc = Base continuous and common, T = Top, Tc = Top continuous and common. EOIS = Earliest Oligocene oxygen Isotope Shift.

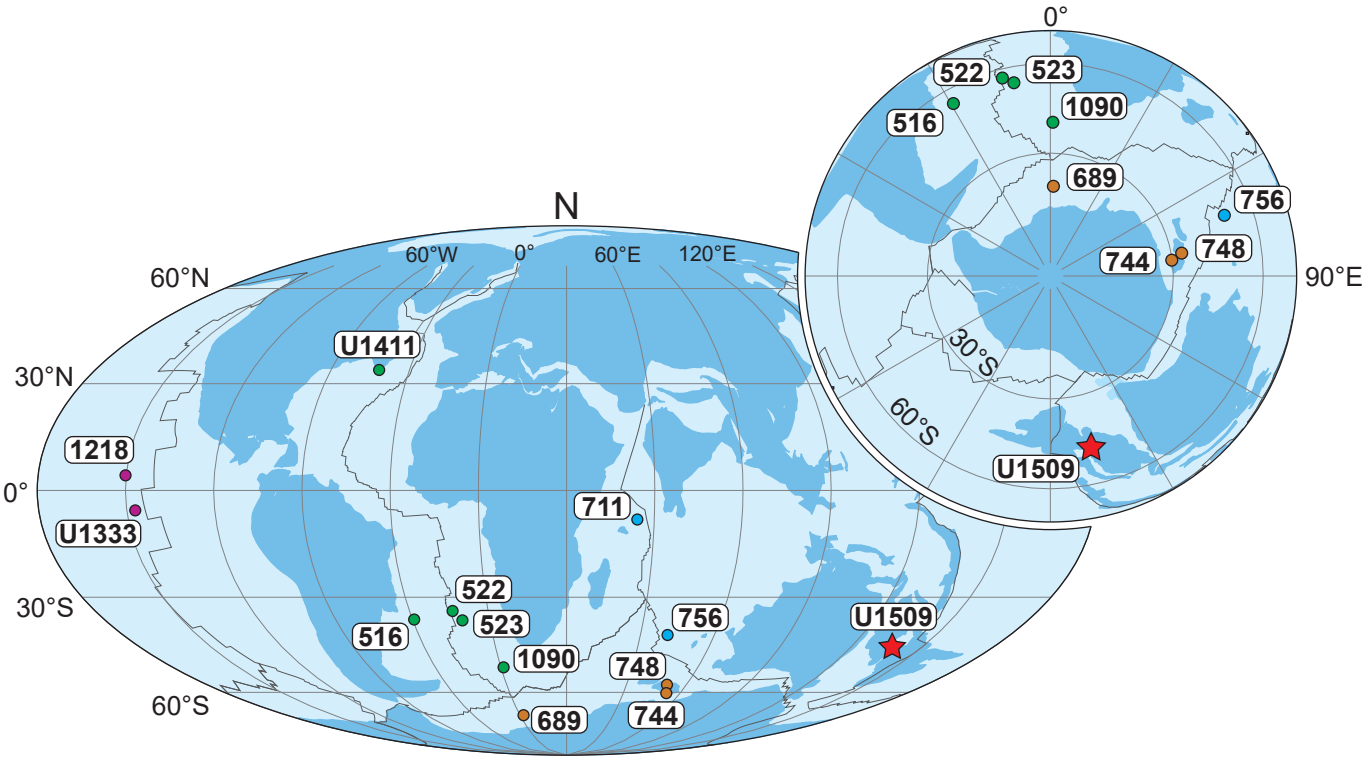
N
60°W
0°
60°E
120°E
60°N
30°N
0°
30°S
60°S
U1411
1218
U1333
711
522
523
516
1090
748
744
689
756
U1509
0°
90°E
30°S
60°S

Figure 1

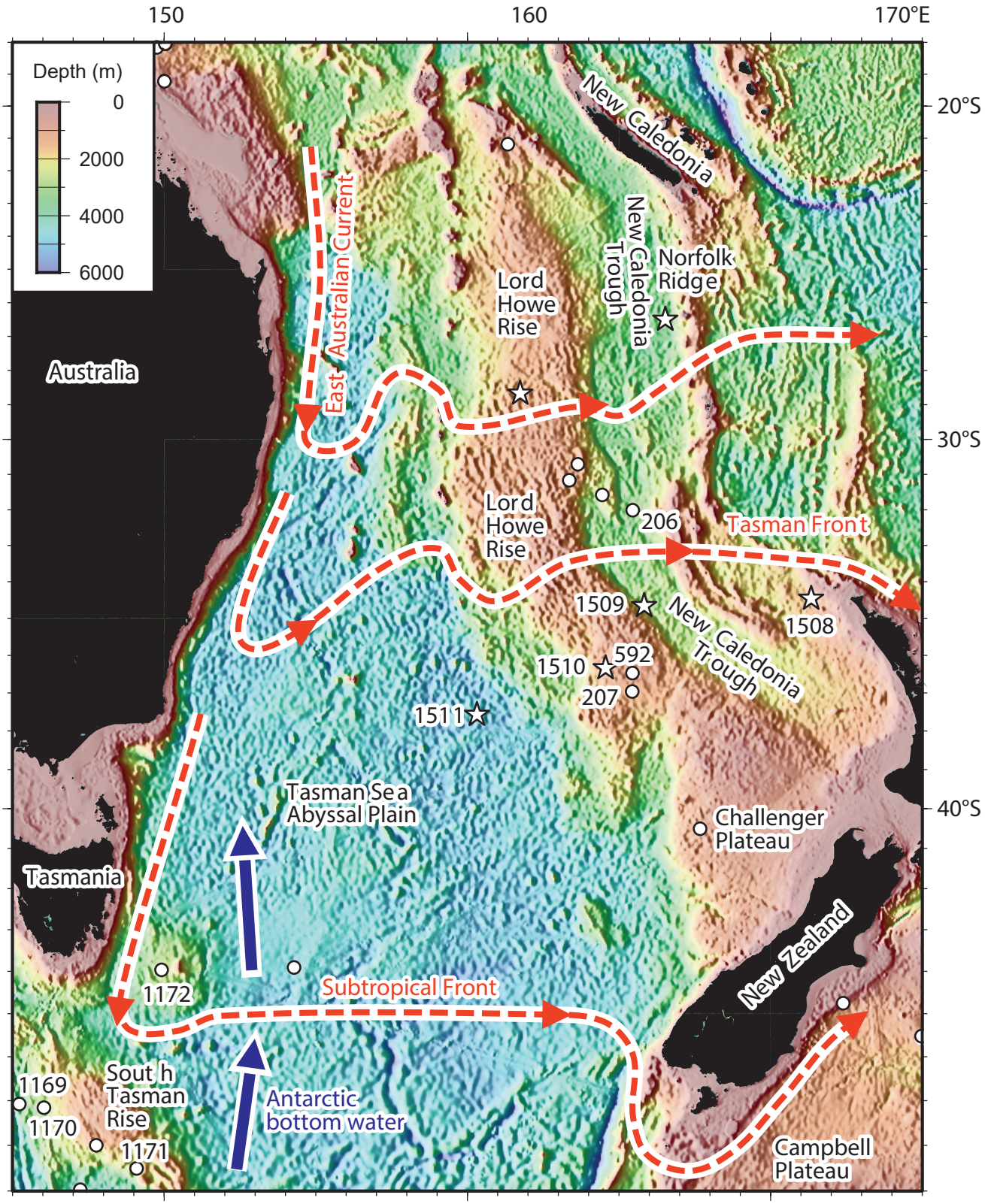
150
160
170°E
20°S
30°S
40°S
Depth (m)
0
2000
4000
6000
New Caledonia
East Australian Current
New Caledonia Trough
Norfolk Ridge
Lord Howe Rise
Australia
Lord Howe Rise
206
Tasman Front
1509
1508
New Caledonia Trough
1510
592
207
1511
Tasman Sea Abyssal Plain
Challenger Plateau
Tasmania
New Zealand
1172
Subtropical Front
1169
1170
1171
Sout h Tasman Rise
Antarctic bottom water
Campbell Plateau

Figure 2

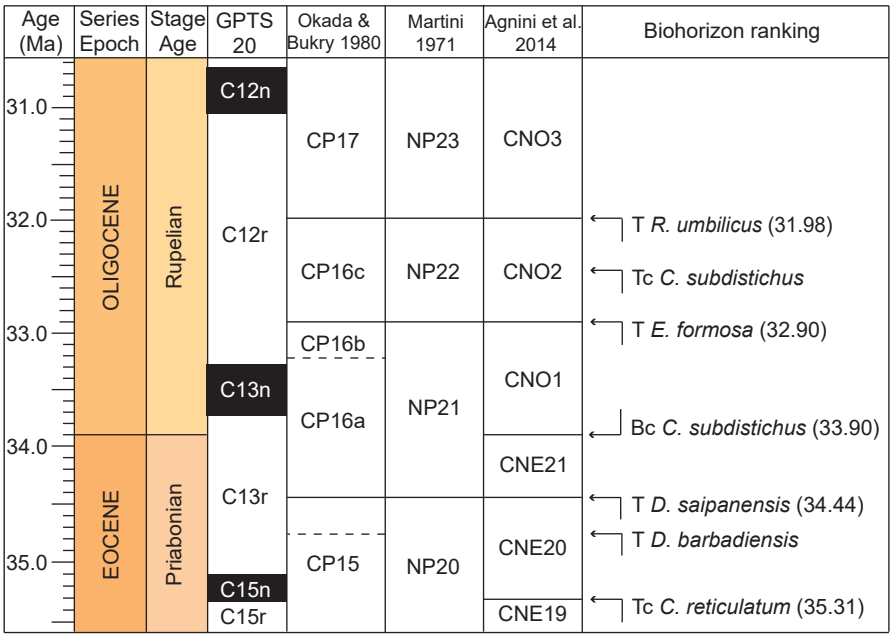
Age (Ma)
Series Epoch
Stage Age
GPTS 20
Okada & Bukry 1980
Martini 1971
Agnini et al. 2014
Biohorizon ranking
31.0
32.0
33.0
34.0
35.0
OLIGOCENE
EOCENE
Rupelian
Priabonian
C12n
C12r
C13n
C13r
C15n
C15r
CP17
CP16c
CP16b
CP16a
CP15
NP23
NP22
NP21
NP20
CNO3
CNO2
CNO1
CNE21
CNE20
CNE19
T R. umbilicus (31.98)
Tc C. subdistichus
T E. formosa (32.90)
Bc C. subdistichus (33.90)
T D. saipanensis (34.44)
T D. barbadiensis
Tc C. reticulatum (35.31)

Figure 3

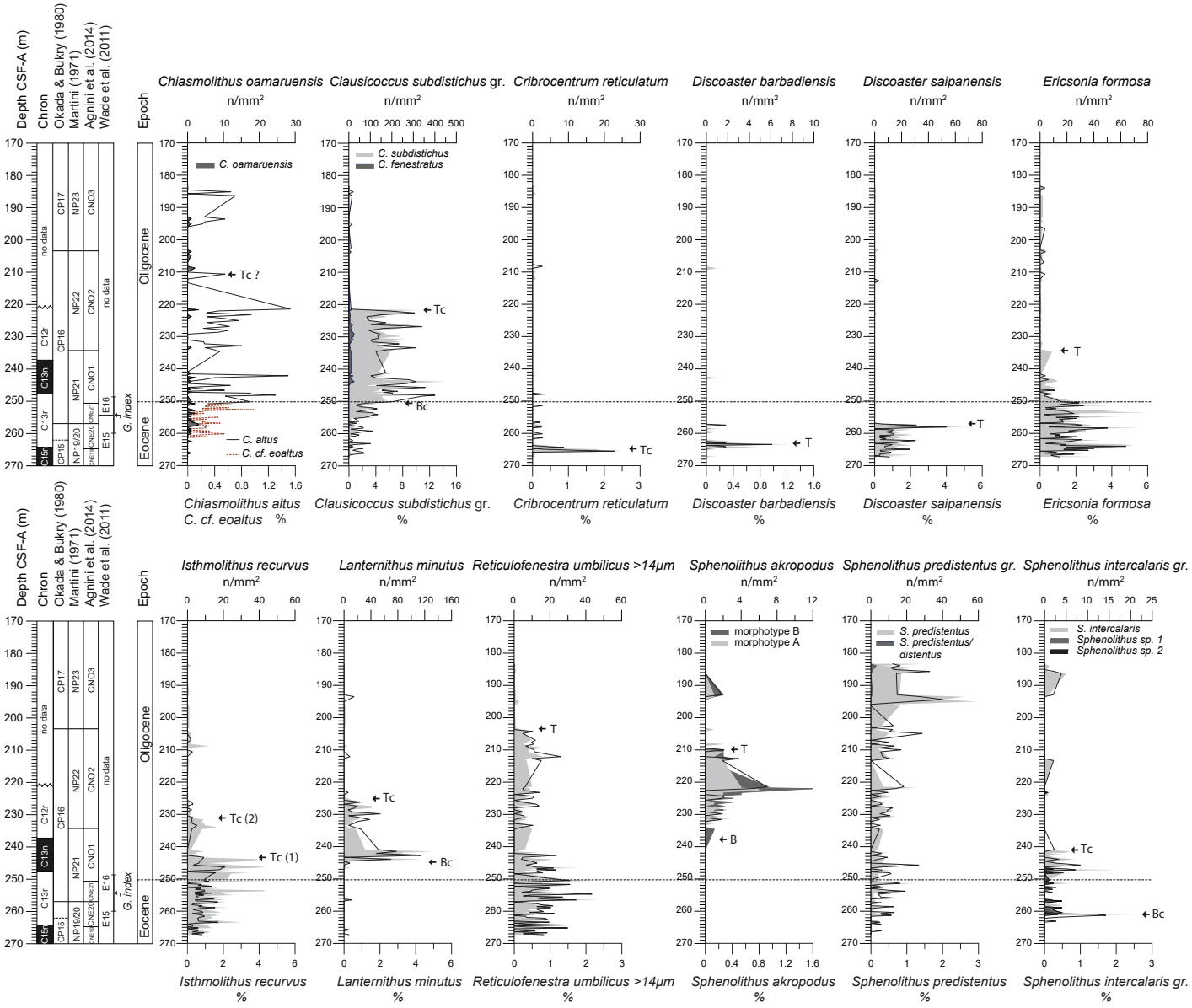
Depth CSF-A (m)
Chron
Okada & Bukry (1980)
Martini (1971)
Agnini et al. (2014)
Wade et al. (2011)
Epoch
Chiasmolithus oamaruensis
Clausicoccus subdistichus gr.
Cribrocentrum reticulatum
Discoaster barbadiensis
Discoaster saipanensis
Ericsonia formosa
n/mm²
C. oamaruensis
Tc ?
C. altus
C. cf. eoaltus
C. subdistichus
C. fenestratus
Tc
Bc
T
Chiasmolithus altus
C. cf. eoaltus %
Clausicoccus subdistichus gr. %
Cribrocentrum reticulatum %
Discoaster barbadiensis %
Discoaster saipanensis %
Ericsonia formosa %
Isthmolithus recurvus
Lanternithus minutus
Reticulofenestra umbilicus >14µm
Sphenolithus akropodus
Sphenolithus predistentus gr.
Sphenolithus intercalaris gr.
Tc (2)
Tc (1)
morphotype B
morphotype A
B
S. predistentus
S. predistentus/ distentus
S. intercalaris
Sphenolithus sp. 1
Sphenolithus sp. 2
Isthmolithus recurvus %
Lanternithus minutus %
Reticulofenestra umbilicus >14µm %
Sphenolithus akropodus %
Sphenolithus predistentus %
Sphenolithus intercalaris gr. %

Figure 4

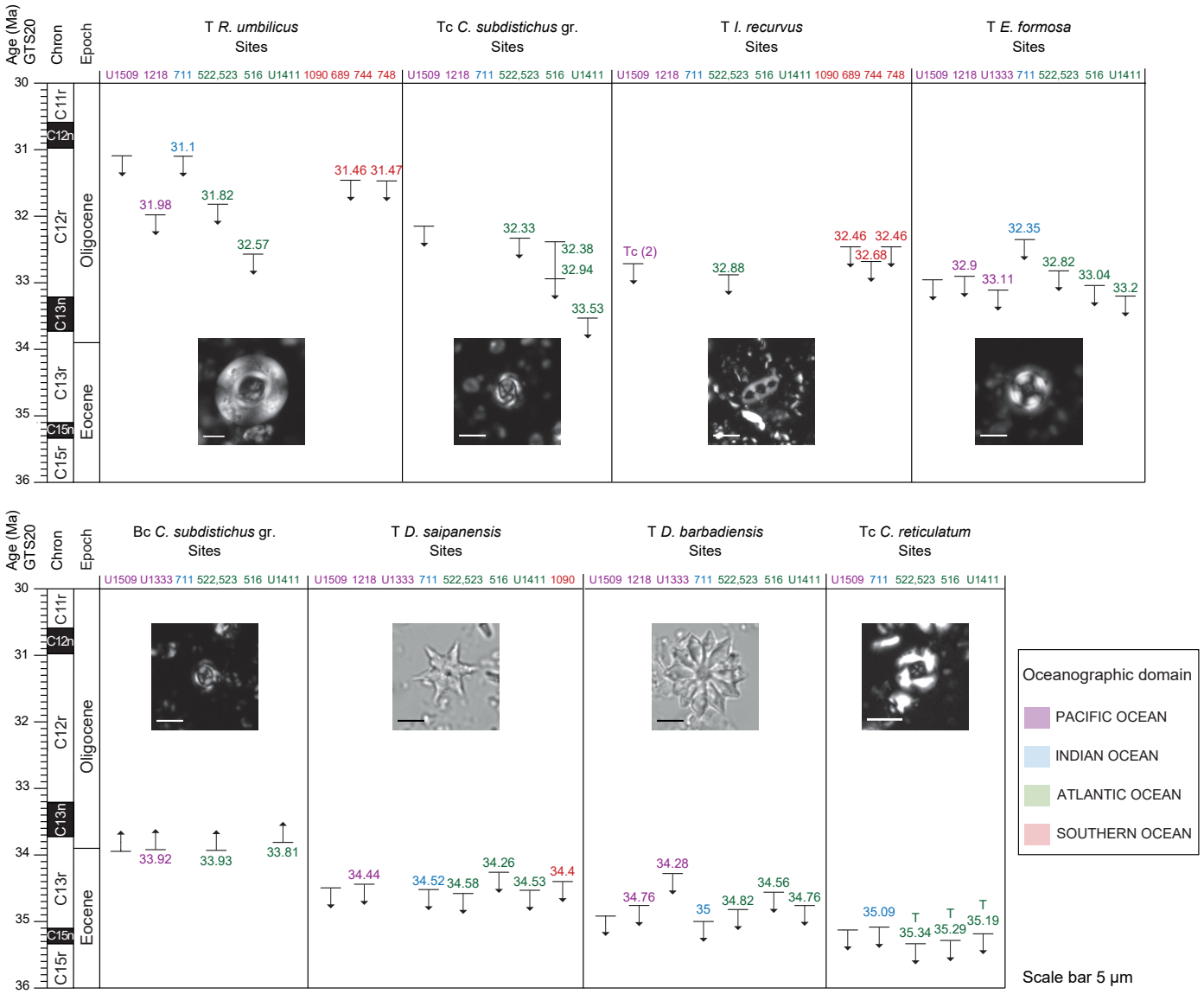
Age (Ma) GTS20
Chron
Epoch
T R. umbilicus Sites
Tc C. subdistichus gr. Sites
T I. recurvus Sites
T E. formosa Sites
U1509 1218 711 522,523 516 U1411 1090 689 744 748
U1509 1218 711 522,523 516 U1411
U1509 1218 U1333 711 522,523 516 U1411
C11r
C12n
C12r
C13n
C13r
C15n
C15r
Oligocene
Eocene
30
31
32
33
34
35
36
31.1
31.98
31.82
32.57
31.46 31.47
32.33
32.38
32.94
33.53
Tc (2)
32.88
32.46 32.46
32.68
32.35
32.9
33.11
32.82
33.04
33.2
Bc C. subdistichus gr. Sites
T D. saipanensis Sites
T D. barbadiensis Sites
Tc C. reticulatum Sites
U1509 U1333 711 522,523 516 U1411
U1509 1218 U1333 711 522,523 516 U1411 1090
U1509 1218 U1333 711 522,523 516 U1411
U1509 711 522,523 516 U1411
33.92
33.93
33.81
34.44
34.52 34.58
34.26
34.53
34.4
34.76
34.28
35
34.82
34.56
34.76
35.09
T 35.34
T 35.29
T 35.19
Oceanographic domain
PACIFIC OCEAN
INDIAN OCEAN
ATLANTIC OCEAN
SOUTHERN OCEAN
Scale bar 5 µm

Figure 5

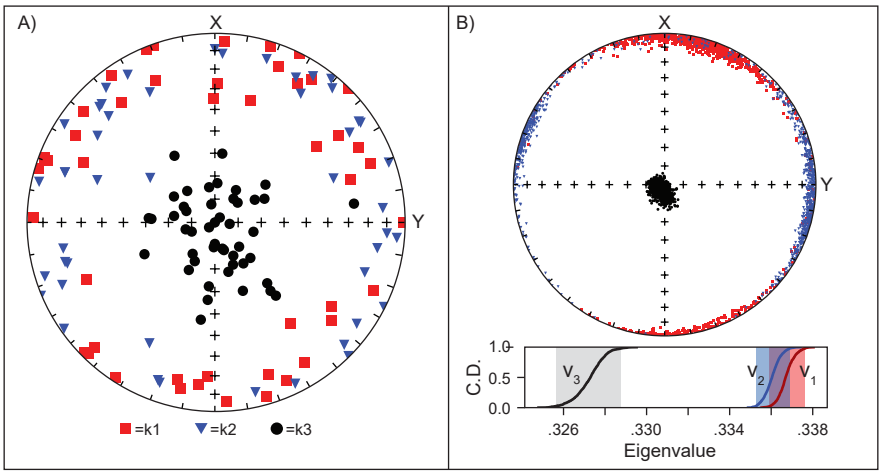

Figure 6

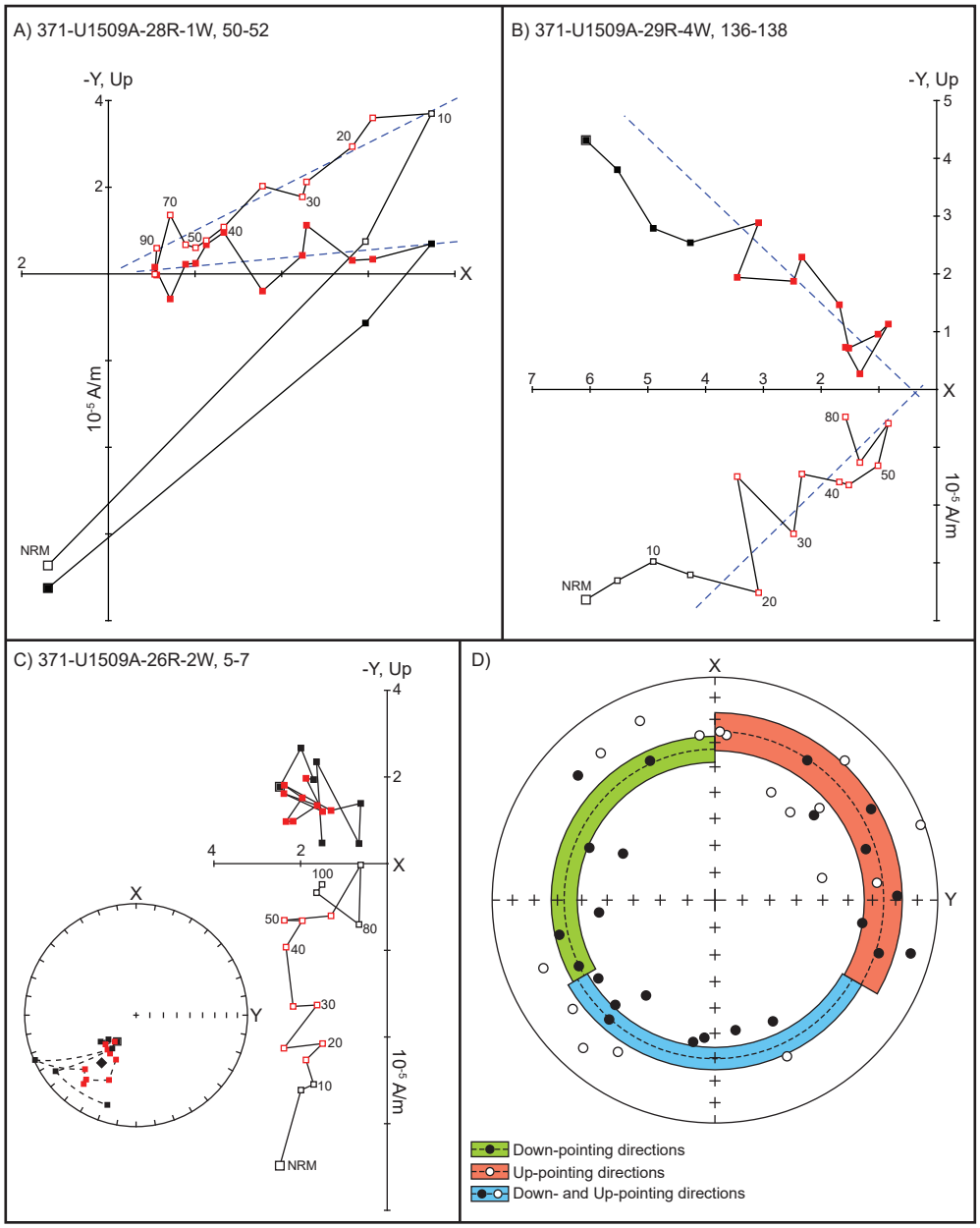
A) 371-U1509A-28R-1W, 50-52
-Y, Up
X
10⁻⁵ A/m
NRM
B) 371-U1509A-29R-4W, 136-138
-Y, Up
X
10⁻⁵ A/m
NRM
C) 371-U1509A-26R-2W, 5-7
-Y, Up
X
Y
10⁻⁵ A/m
NRM
D)
X
Y
Down-pointing directions
Up-pointing directions
Down- and Up-pointing directions

Figure 7

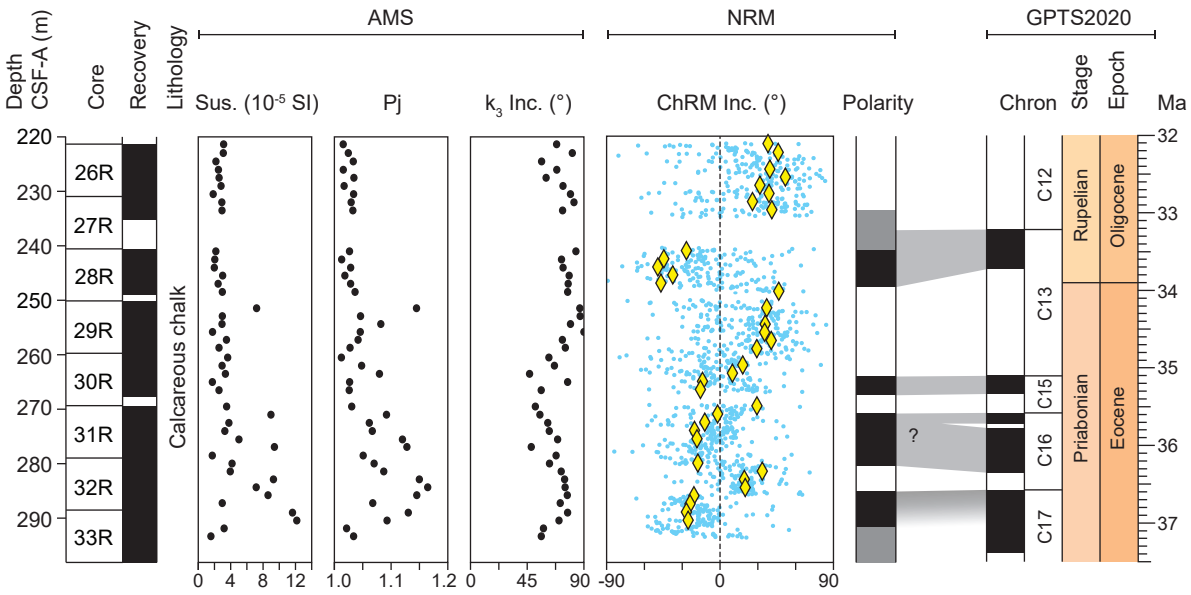
Depth CSF-A (m)
Core
Recovery
Lithology
AMS
Sus. (10-5 SI)
Pj
k3 Inc. (°)
NRM
ChRM Inc. (°)
Polarity
GPTS2020
Chron
Stage
Epoch
Ma
220
230
240
250
260
270
280
290
26R
27R
28R
29R
30R
31R
32R
33R
Calcareous chalk
0 4 8 12
1.0 1.1 1.2
0 45 90
-90 0 90
?
C12
C13
C15
C16
C17
Rupelian
Priabonian
Oligocene
Eocene
32
33
34
35
36
37

Figure 8

DSDP/ ODP/IODP	Location	Latitude	Longitude	Water depth (m)	Paleodepth (m)	Reference
Site U1509	New Caledonia Trough, Pacific Ocean	34°39.13'S	165°49.66'E	2911	lower bathyal	Sutherland et al. (2019)
Site 1218	Eastern Equatorial Pacific	8°53.378'N	135°22.00'W	4826	~3700–4300	Blaj et al. (2009)
Site U1333	Eastern Equatorial Pacific	10°30.996'N	138°25.159'W	4853	lower bathyal to abyssal	Toffanin et al. (2013)
Site 711	Equatorial Indian Ocean	2°44.56'S	61°09.78'E	4428	~3450-3750	Fioroni et al. (2015)
Site 756	Ninetyeast Ridge (Indian Ocean)	27°21.25'S	87°35.89'E	1516	~400	Viganò et al. (2023)
Site U1411	Newfoundland Ridge (NW Atlantic)	41°37'N	48°6'W	3300	~2800	Newsam (2017)
Site 522	Walvis Ridge (SE Atlantic)	26°6.843'S	5°7.748'W	4441	~3000	Backman (1987)
Site 523	Walvis Ridge (SE Atlantic Ocean)	28°33.131'S	2°15.078'W	4562	~3450-3550	Backman (1987)
Site 516	Rio Grande Rise (SW Atlantic Ocean)	30°16.59'S	35°17.10'W	1313	middle bathyal	Wei and Wise (1989)
Site 1090	Agulhas Ridge (SE Atlantic Ocean)	42°54'S	8°53'E	3702	~3000-3300	Marino and Flores (2002)
Site 689	Maud Rise (Southern Ocean)	64°31.009'S	03°06.026'E	2080	~1500-2000	Persico and Villa (2004)
Site 744	Kerguelen Plateau (Southern Ocean)	61°34.66'S	80°35.46'E	2307	~2250	Persico and Villa (2004)
Site 748	Kerguelen Plateau (Southern Ocean)	58°26.45'S	78°58.89'E	1291	~1200	Villa et al. (2008)

Table 1

Table 2

Event	Taxon/Chron	Top sample (hole-core-section,cm)	Base sample (hole-core-section,cm)	Top depth (CSF-A, m)	Base depth (CSF-A, m)	Mid point (CSF-A, m)	Error (± m)	Depth error (m)	Chron	From Top Chron	Age (Ma) GTS20	Sampling error (Myr)	Age (Ma)
B	**C12n**									1.000	**30.98**		
T	*Reticulofenestra umbilicus*	U1509A-23R-1W, 100-101	U1509A-23R-2W, 8-9	203.11	203.69	203.40	0.29	0.58	C12r	0.259		0.028	31.08
T	*Sphenolithus akropodus*	U1509A-24R-2W, 132-133	U1509A-24R-3W, 42-43	209.41	210.01	209.71	0.30	0.60	C12r	0.397		0.029	31.46
Tc	*Chiasmolithus altus*	U1509A-24R-3W, 42-43	U1509A-24R-3W, 102-103	210.01	210.61	210.31	0.30	0.60	C12r	0.410		0.029	31.50
Tc	*Clausicoccus subdistichus*	U1509A-26R-1W, 11-12	U1509A-26R-2W, 2-3	221.42	221.71	221.56	0.14	0.29	C12r	0.656		0.014	32.17
Tc	*Lanternithus minutus*	U1509A-26R-3W, 122-123	U1509A-26R-4W, 32-33	224.41	225.01	224.71	0.30	0.60	C12r	0.725		0.029	32.36
Tc (2)	*Isthmolithus recurvus*	U1509A-26R-8W, 15-16	U1509A-26R-8W, 45-46	230.41	230.71	230.56	0.15	0.30	C12r	0.853		0.015	32.71
T	*Ericsonia formosa*	U1509A-27R-3W, 9-10	U1509A-27R-3W, 70-71	234.00	234.61	234.30	0.31	0.61	C12r	0.935		0.030	32.94
B	**C12r**	U1509A-27R-2W, 110-112	U1509A-28R-1W, 50-52	233.51	241.01	237.26	3.75	7.50		1.000	**33.21**	0.367	
B	*Sphenolithus akropodus*	U1509A-27R-3W, 70-71	U1509A-28R-1W, 40-41	234.61	240.91	237.76	3.15	6.30	C13n	0.047		0.308	33.15
Tc	*Sphenolithus intercalaris*	U1509A-28R-1W, 40-41	U1509A-28R-1W, 100-101	240.91	241.51	241.21	0.30	0.60	C13n	0.377		0.029	33.37
Tc (1)	*Isthmolithus recurvus*	U1509A-28R-2W, 130-131	U1509A-28R-3W, 40-41	243.31	243.91	243.61	0.30	0.60	C13n	0.607		0.029	33.50
Bc	*Lanternithus minutus*	U1509A-28R-3W, 40-41	U1509A-28R-3W, 100-101	243.91	244.51	244.21	0.30	0.60	C13n	0.664		0.029	33.53
T	EOIS	U1509A-28R-5W, 20-21	U1509A-28R-5W, 50-51	246.00	246.90	246.75	0.15	0.90	C13n	0.907		0.044	33.66
B	**C13n**	U1509A-28R-5W, 56-58	U1509A-28R-6W, 56-58	246.97	248.47	247.72	0.75	1.50		1.000	**33.73**	0.073	
Bc	*Clausicoccus subdistichus*	U1509A-29R-1W, 40-41	U1509A-29R-1W, 9-10	250.20	250.51	250.35	0.16	0.31	C13r	0.159		0.026	33.95
T	*Discoaster saipanensis*	U1509A-29R-5W, 67-68	U1509A-29R-5W, 96-97	256.82	257.11	256.96	0.15	0.29	C13r	0.559		0.024	34.50
Bc	*Sphenolithus intercalaris*	U1509A-30R-1W, 130-131	U1509A-30R-2W, 9-10	261.01	261.30	261.15	0.15	0.29	C13r	0.812		0.024	34.84
T	*Discoaster barbadiensis*	U1509A-30R-2W, 70-71	U1509A-30R-2W, 100-101	261.91	262.21	262.06	0.15	0.29	C13r	0.867		0.025	34.92
T	**C15n**	U1509A-30R-3W, 105-107	U1509A-30R-4W, 105-107	263.51	265.01	264.26	0.75	1.50		1.000	**35.10**	0.125	
Tc	*Cribrocentrum reticulatum*	U1509A-30R-4W, 65-66	U1509A-30R-4W, 95-96	264.61	264.91	264.76	0.15	0.30	C15n	0.132		0.019	35.13
T	**C15r**	U1509A-30R-6W, 0-2	U1509A-31R-1W, 20-22	266.51	269.51	268.01	1.50	3.00		1.000	**35.34**	0.187	